High-spin states in doubly odd ^{176}Re and signature inversion in $\pi h_{9/2} \otimes \nu i_{13/2}$ structures

M. A. Cardona,[1,2] A. J. Kreiner,[1,2,4] D. Hojman,[1,2,4] G. Levinton,[1] M. E. Debray,[1,2] M. Davidson,[3,4] J. Davidson,[3,4] R. Pirchio,[3] H. Somacal,[1,2] D. R. Napoli,[5] D. Bazzacco,[6] N. Blasi,[7] R. Burch,[5] D. De Acuña,[5] S. M. Lenzi,[6] G. Lo Bianco,[7] J. Rico,[5] and C. Rossi Alvarez[6]

[1]*Departamento de Física, Comisión Nacional de Energía Atómica, 1429 Buenos Aires, Argentina*

[2]*Escuela de Ciencia y Tecnología, Universidad de San Martín, 1650 San Martín, Argentina*

[3]*Departamento de Física, Facultad de Ciencias Exactas y Naturales, Universidad de Buenos Aires, Buenos Aires, Argentina*

[4]*CONICET, 1033 Buenos Aires, Argentina*

[5]*INFN, Laboratori Nazionali di Legnaro, Legnaro, Italy*

[6]*Dipartimento di Fisica, Sezione di Padova, Padova, Italy*

[7]*Dipartimento di Fisica and INFN, Sezione di Milano, Milano, Italy*

(Received 17 August 1998)

High-spin states in doubly odd ^{176}Re were investigated by means of in-beam γ-ray spectroscopy techniques using the multidetector array GASP. Excited states of ^{176}Re were populated using the ^{165}Ho(^{16}O,5n) reaction at a beam energy of 101 MeV. Seven rotational bands have been observed and their configurations have been discussed. Alignments, band crossing frequencies, and electromagnetic properties have been analyzed in the framework of the cranking model. Signature inversion phenomena in the $\pi h_{11/2} \otimes \nu i_{13/2}$ and $\pi h_{9/2} \otimes \nu i_{13/2}$ structures are discussed. In the latter case signature inversion is traced to a large repulsive matrix element of the $p-n$ force acting in the maximally aligned $J=11$ state. [S0556-2813(99)04702-0]

PACS number(s): 21.10.Re, 21.60.Ev, 23.20.Lv, 27.70.+q

I. INTRODUCTION

The study of doubly odd nuclei has provided, for about two decades now [1], a fruitful ground for the discovery and discussion of a number of interesting nuclear structure phenomena. One recurrent theme [1–3] has been the attempt to establish a general classification scheme for the coupling modes of two nonidentical valence nucleons, leading to semidecoupled [1,4], doubly decoupled [4,5], and compressed structures [2]. A particularly interesting phenomenon discovered along the way was that of signature inversion [6,7]. The present study of the doubly odd nucleus ^{176}Re is framed into the above context. It has been reexamined using the GASP detector array at the Legnaro Tandem Facility yielding a wealth of rotational structures where the above-mentioned ideas can be tested. In particular a signature inversion is found at high spins in the $\pi h_{9/2} \otimes \nu i_{13/2}$ semidecoupled structure, a feature recently discovered in ^{162,164}Tm and ^{174}Ta [8,9] and its origin discussed in terms of the experimental proton-neutron force present in ^{208}Bi [10].

A partial study concerning the doubly decoupled band in ^{176}Re has already been published [11] and preliminary results of the level scheme have been reported earlier [12].

II. EXPERIMENTS AND RESULTS

A. Measurements

High-spin states of ^{176}Re were populated through the ^{165}Ho(^{16}O,5n) reaction at 101 MeV. The target consisted of a 2 mg/cm^2 Ho rolled foil, backed with a 1.5 mg/cm^2 evaporated Bi layer. The beam was provided by the Tandem XTU accelerator of Legnaro and γ-rays emitted by the evaporation residues were detected using the GASP array [13], which consisted for this coincidence experiment of 39 Compton suppressed large volume Ge detectors, a planar detector and a multiplicity filter of 80 bismuth germanate (BGO) elements, providing the sum-energy and γ-ray multiplicity used to select the different reaction channels. Events were collected when at least three suppressed Ge and three inner multiplicity filter detectors were fired. With this condition a total of 10^9 events were recorded. The data corresponding to Ge energies (E_γ) were sorted into fully symmetrized matrices and cubes. The large number of triple coincidences offered the possibility to generate matrices gated by transitions of the different bands of ^{176}Re and to obtain very clean double-gated spectra. A nonsymmetrized matrix of the planar against all the large volume Ge detectors was very useful to examine the low-energy region of the spectra with the high-energy resolution of the planar detector. Known bands in ^{176}Re [14] were extended up to ≈ 28–$29\hbar$, and the assignment of new bands to ^{176}Re was based on coincidence data, multiplicity distributions, coincidences with Re K x rays and the knowledge of the neighboring Re isotopes. The most intensely populated nuclei were ^{175,176,177}Re [15–17], ^{175,176}W [15,16], and ^{173}Ta [18] corresponding to the $6n$, $5n$, $4n$, $5np$, $4np$, and $\alpha 3n$ channels, respectively. In the off-line analysis of the data the $5n$ channel leading to ^{176}Re was enhanced by setting a proper gate on the multiplicity spectrum of the BGO ball. A matrix of γ-ray energy in the Ge detectors vs BGO multiplicity was used to find assignments of γ transitions to different reaction products. Figure 1 shows the BGO multiplicity spectra obtained by setting gates on pure transitions belonging to ^{177}Re, ^{176}Re, and ^{175}Re. In the spectra the mean value of the multiplicity distribution is indicated, the variation of the average multiplicity with the number of evaporated neutrons is apparent. According to this analysis and to the coincidence with Re K x rays, the 320.3 and the 504.1 keV transitions were assigned to ^{176}Re [Figs. 1(c) and 1(d)]. The Ge times ($t\gamma$) were measured with respect to the fast signal provided by the multiplicity filter. For each Ge detector a matrix $E\gamma$

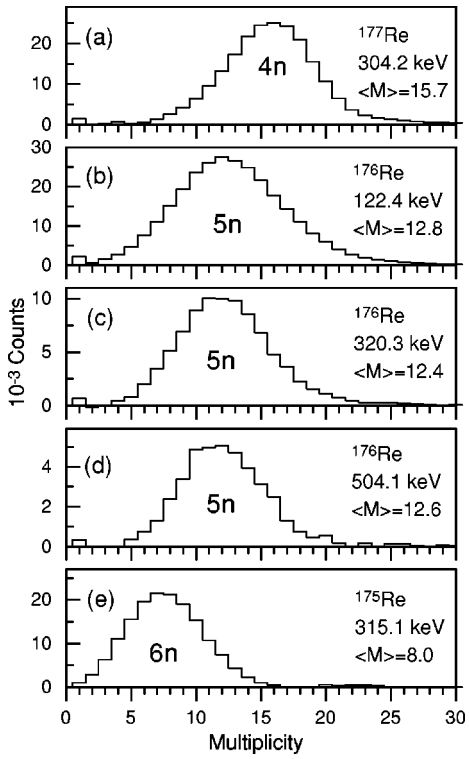

FIG. 1. Multiplicity distribution of neutron channels in the reaction ^{165}Ho+ ^{16}O at 101 MeV, obtained by gating on strong and clean lines: $4n$, 304.2 keV (a) belonging to ^{177}Re; $5n$, 122.4 (b) of ^{176}Re (known from previous work, Ref. [14]) and 320.3 (c) and 504.1 keV (d) also assigned to ^{176}Re; and $6n$, 315.1 keV (e) belonging to ^{175}Re. In each spectrum the average multiplicity is indicated.

vs $t\gamma$ was constructed. The fast-time response obtained with the small volume planar detector was useful to search for delayed transitions. In order to extract information on multipolarity of γ transitions, to aid the assignment of spins and parities to the level scheme, the data were sorted to allow a directional correlation orientation (DCO) analysis. For this purpose a nonsymmetrized matrix using the detectors at $\theta_2 = 90°$ with respect to the beam direction against those at $\theta_1 = 31.7°$, $36°$, $144°$, and $148.3°$ was constructed. In the GASP geometry, setting gates on stretched quadrupole transitions, leads to theoretical DCO ratios $I\gamma_{\text{gate}=\theta_2}(\theta_1)/I\gamma_{\text{gate}=\theta_1}(\theta_2) \approx 1$ for stretched quadrupole transitions and ≈ 0.6 for pure dipole ones.

B. Level scheme of ^{176}Re

The level scheme of ^{176}Re deduced from the data obtained here is shown in Fig. 2. Figures 3, 7, and 10 show summed coincidence spectra of the large volume Ge detectors gated on pairs of transitions belonging to the same band or to two different bands (to enhance the linking transitions between them). In Fig. 3(a) the lines belonging to band A are indicated. The low-lying dipole transitions of band A have already been assigned to ^{176}Re [14]. In the present work we extended this band up to $28\hbar$ and added the $E2$ crossover transitions. The order of the 70.5 and the 99.5 keV lines has been changed as discussed below. Figure 4(a) shows a coincidence spectrum of the planar detector obtained setting a gate on the 160.9 keV γ ray. In this spectrum, assuming the level scheme proposed in the present work, the intensity of the 99.5 keV compared with that of the 122.4 keV implies a total conversion coefficient, $\alpha_T = 0.36(9)$, which agrees with the theoretical value $\alpha_T = 0.39$ expected for an $E1$ multipolarity [19], confirming the 99.5 keV as an out-of-band transition having $E1$ character and depopulating the bandhead level of band A which is an isomeric state. The time spectrum obtained setting a gate on the 99.5 keV in the planar detector is shown in Fig. 5, together with the best fit through the experimental points. The fit was made using an exponential decay folded with the prompt spectrum extracted from the 91.9 keV line (assigned to band E of ^{176}Re) and a half-

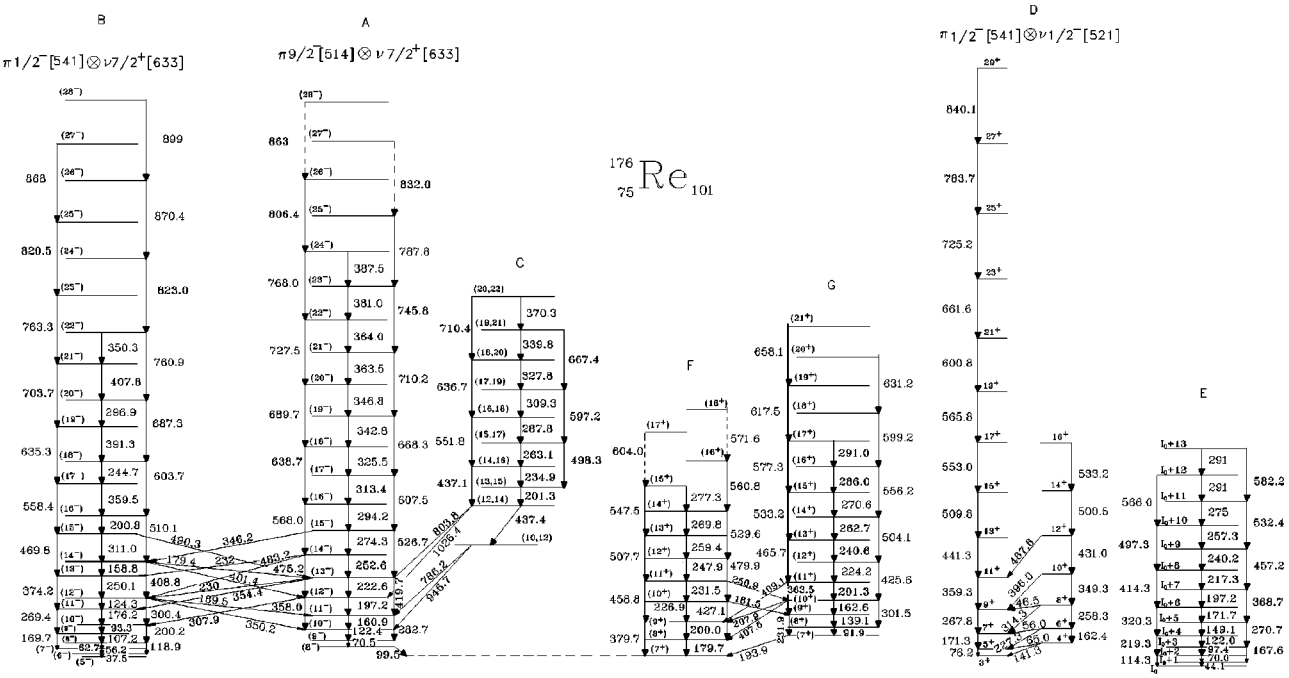

FIG. 2. Level scheme of ^{176}Re proposed in the present work.

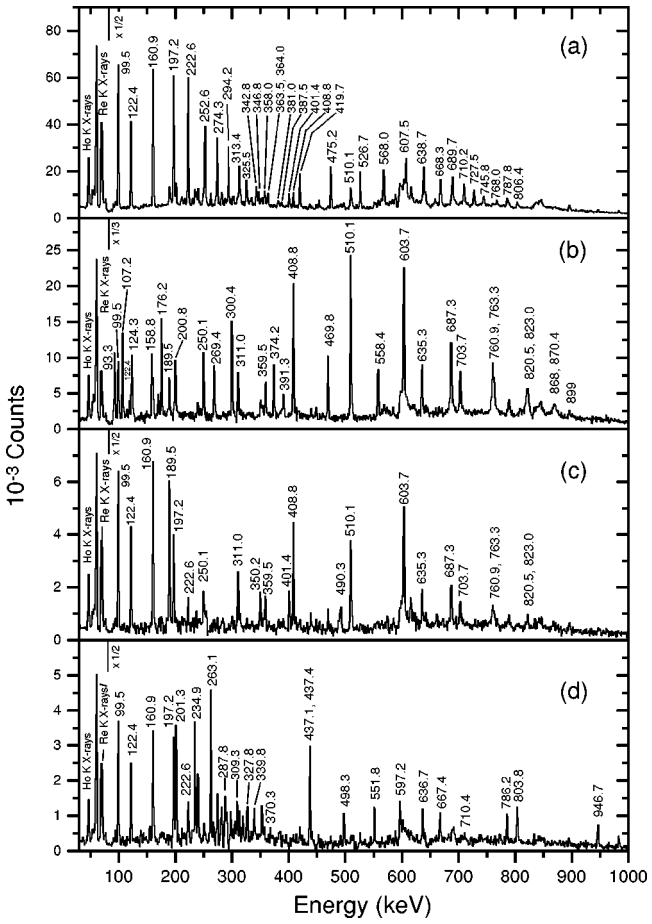

FIG. 3. γ-ray coincidence spectra of Ge detectors corresponding to the sum of several gates on pairs of transitions: (a) both belonging to band A; (b) both belonging to band B; (c) one below the (11^-) of band A and the other above the (12^-) of band B; (d) one of band C and the other of band A below the (12^-) state.

life of $T_{1/2}=30(3)$ ns was determined. Assuming the isomeric state to be fully depopulated through the 99.5 keV $E1$ transition a $B(E1,99.5\ \text{keV})=5.3(5)\times10^{-6}$ W.u. (corrected by internal conversion) is estimated for this decay. The angular distribution of the 99.5 keV is probably attenuated due to the isomeric lifetime and its DCO value of 0.90(3) did not allow to discriminate between a $\Delta I=0$ or $\Delta I=1$ transition. Figure 4(a) shows the 70.5 keV line, which is in coincidence with transitions of band A and has a time spectrum showing only a prompt component. From intensity balance a total conversion coefficient $\alpha_T=3.0(4)$ was estimated for the 70.5 keV, consistent with an $M1(E2)$ multipolarity (see Table I) with mixing ratio $|\delta|=0.16(8)$. Due to these facts the 70.5 keV line was placed in band A above the isomer. However, if the 70.5 keV belongs to band A, the crossover transition, 122.4 keV+70.5 keV=192.9 keV should be present, but it was not observed. The expected intensity of the 192.9 keV was estimated assuming for the (10^-) state of band A a $B(M1)/B(E2)$ value equal to that of the (11^-) state and was found to be below the detection limit of the experiment.

The coincidence spectrum of Fig. 3(b) shows transitions belonging to band B. Around spin $12\hbar-15\hbar$, levels in bands A and B lie very close in energy caused by accidental degeneracies. This leads to the mixing of several states of both

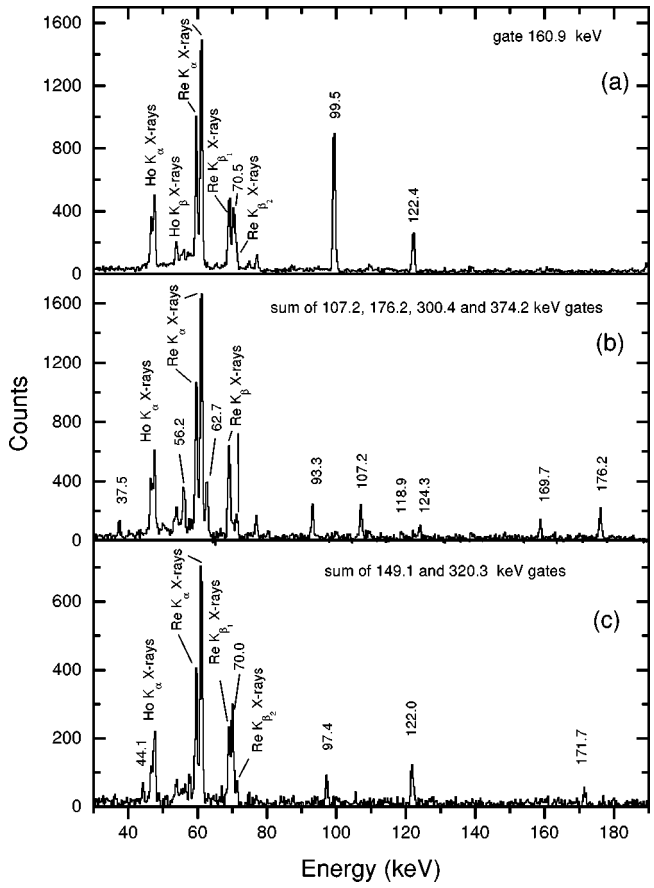

FIG. 4. Planar coincidence spectra obtained with gate or sum of gates on selected transitions of bands A (a), B (b), and E (c).

structures. Figure 3(c) shows a summed coincidence spectrum gated on pairs of transitions, one below the (11^-) state of band A and the other above the (12^-) of band B, to emphasize the linking transitions from band B to band A. The connections fix unambiguously spin and parity of one band relative to the other. The low-lying 37.5, 56.2, and 62.7 keV transitions of band B are very well resolved in the spectrum of the planar detector gated on some strong lines of the band [Fig. 4(b)], and from the intensity balance an almost

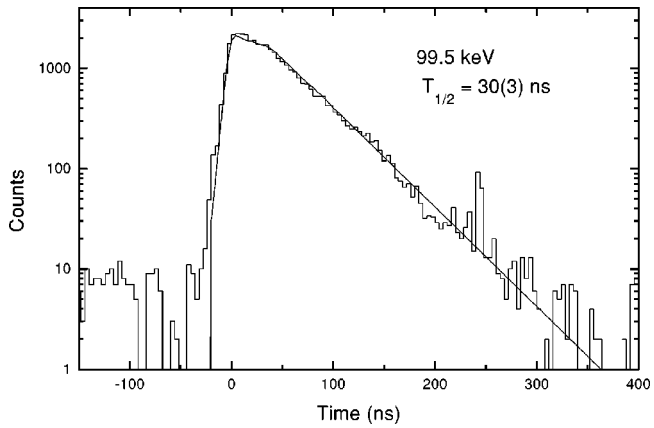

FIG. 5. Time distribution of the 99.5 keV line corresponding to the decay of the (8^-) level, bandhead of band A, arising from the BGO multiplicity filter and planar detector coincidence. The best fit through the data points is also shown.

TABLE I. Total internal conversion coefficients for low-energy transitions in ^{176}Re. The experimental values α_T^{exp} were obtained from intensity balance and the theoretical values α_T^{th} from Ref. [19].

E_γ(keV)	Band	α_T^{exp}	α_T^{th}			Assigned multipolarity
			$E1$	$E2$	$M1$	
56.0	D	6(3)	0.36	53.4	5.07	$M1(E2)$
65.0	D	6.0(5)	0.24	26.0	3.28	$M1(E2)$
70.5	A	3.0(4)	0.17	18.0	3.62	$M1(E2)$
76.2	D	13(1)	0.78	13.2	11.9	$E2$
99.5	(a)	0.36(9)	0.39	4.29	5.49	$E1$

[a]Transition depopulating band A.

pure $M1$ multipolarity was obtained for these transitions.

Lines assigned to band C are shown in Fig. 3(d) in addition to γ rays which depopulate band C into band A, and the low-lying lines of band A. For the out-of-band transition of 803.8 keV the DCO was evaluated setting a gate on the quadrupole transition (13^-) to (11^-) of 419.7 keV. A comparison of experimental and calculated DCO ratios establishes for the level depopulated by the 803.8 keV two possible spin values: $I=12$ and $I=14$ (Fig. 6).

States of band D below spin 17^+ have been reported previously [11]. In the present work we show band D up to spin 29^+. In Fig. 7(a) lines assigned to the favored ($\alpha=1$) sequence are shown. In Fig. 7(b) lines of the unfavored ($\alpha=0$) component and connections between the two signatures are indicated. The low-energy transitions of 56.0, 65.0, and 76.2 keV are shown in Fig. 8. For the low-energy highly converted transitions of ^{176}Re intensity balance was used to determine total conversion coefficients, Table I summarizes the experimental values together with the theoretical ones for the total conversion coefficients [19] and the assigned multipolarities. For the 6^+ to 5^+, 227.3 keV transition the DCO ratio was used to determine the $M1(E2)$ mixing ratio (Fig. 9).

No connection was found between bands E, F, and G and the other bands of ^{176}Re. The assignment of these bands to ^{176}Re was based on coincidence with Re K x rays and on multiplicity distributions as mentioned above. In fact the

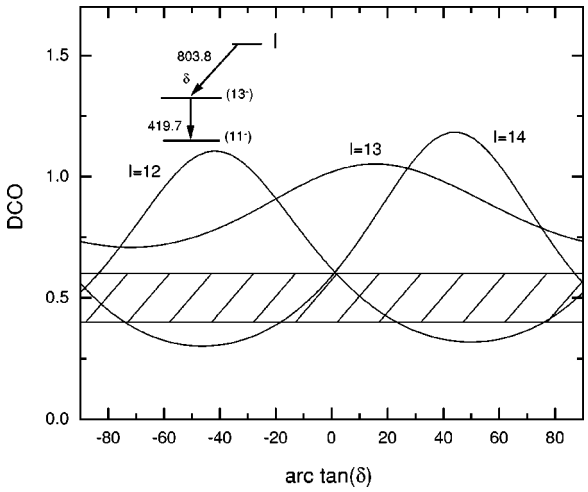

FIG. 6. Comparison of experimental and calculated DCO ratios to determine possible spin values in band C.

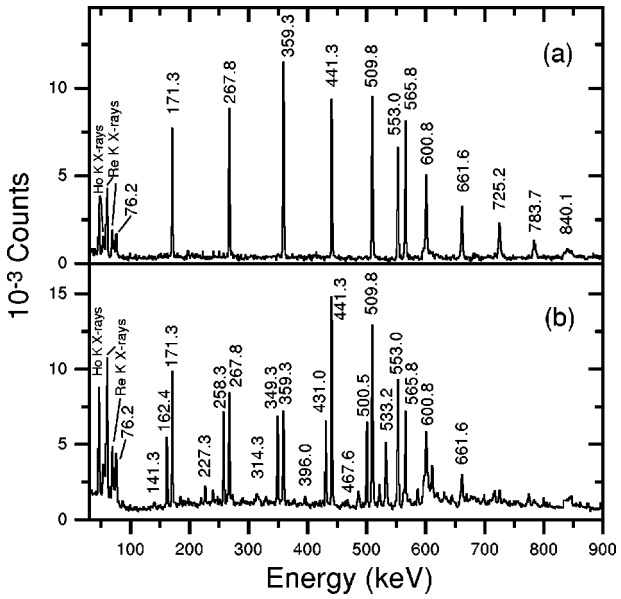

FIG. 7. γ-ray coincidence spectra of Ge detectors corresponding to the sum of several gates on pairs of transitions: (a) of the favored sequence of band D; (b) one of them belonging to the favored and the other to the unfavored sequence of band D, also indicated some of the connections between both sequences.

320.3 and 504.1 keV γ rays of bands E and G, respectively, follow the multiplicity distribution of a five-particle channel [Figs. 1(c) and 1(d)], and besides they are in coincidence with Re K x rays.

In Fig. 10(a) a coincidence γ-ray spectrum with double gates on several pairs of transitions assigned to band E is

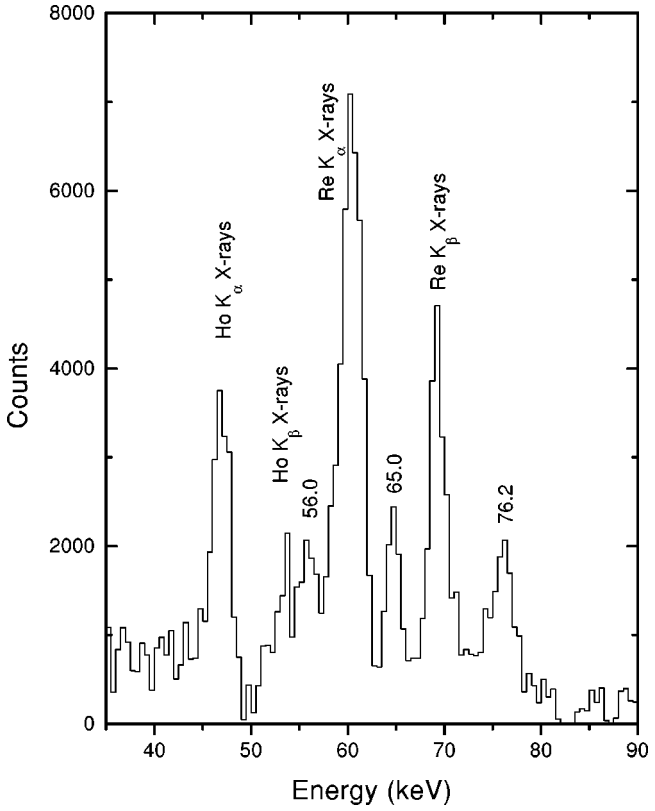

FIG. 8. Low-energy region of coincidence spectrum of the large volume Ge detectors showing transitions of band D.

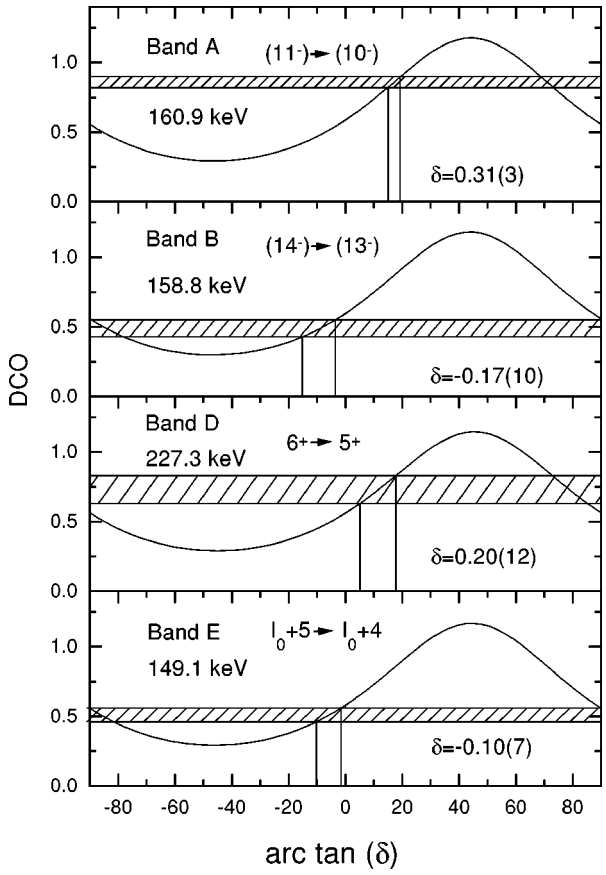

FIG. 9. Experimental and calculated DCO ratios for selected transitions of band A, band B, the 227.3 keV linking both signatures in band D and the 149.1 keV of band E.

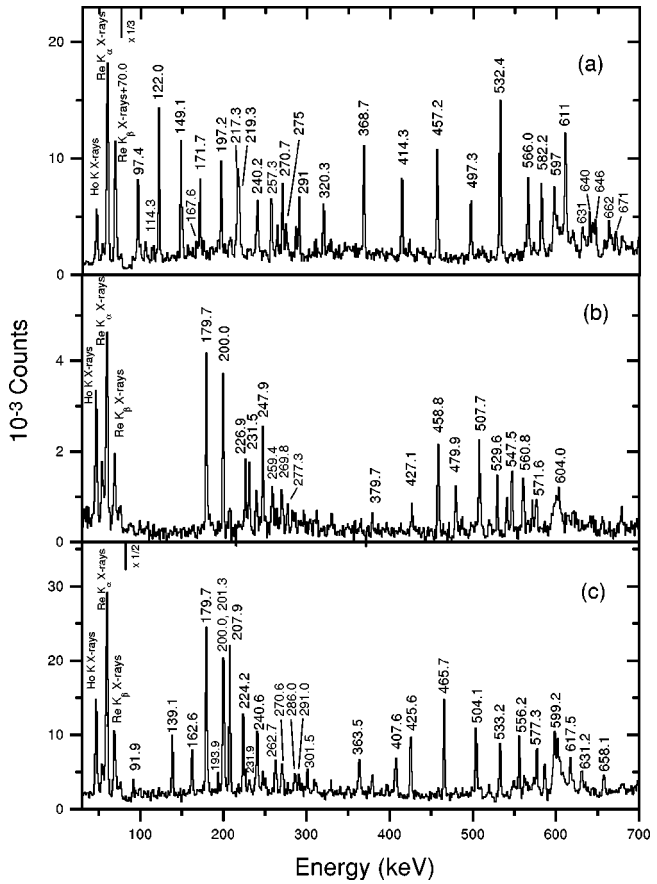

FIG. 10. γ-ray coincidence spectra of Ge detectors corresponding to the sum of several gates on pairs of transitions: (a) of band E; (b) of band F; (c) of band G.

shown. From the data a rotational band with $\Delta I=1$ and crossover transitions was easily constructed up to the I_0+13 level (see Fig. 2). Above this point a number of lines have been observed (597, 611, 631, 640, 646, 662, and 671 keV) in coincidence with γ rays of band E, as can be seen in Fig. 10(a), however they were not indicated on the level scheme because of uncertainties in their placements. The low-energy transitions of 44.1 and 70.0 keV are indicated in the spectrum shown in Fig. 4(c), where the events in the planar detector in coincidence with the 149.1 and 320.4 keV lines have been added. From intensity balance considerations $M1$ multipolarity with the possibility of a small $E2$ admixture was obtained for the 44.1 and the 70.0 keV transitions. The 70.0 keV line is very close in energy to the Re K_β x rays (69.2 and 71.2 keV) and the peaks are not resolved with the large volume Ge detectors [Fig. 10(a)], however the presence of the 70.0 keV peak is evident in Fig. 10(a) from intensity considerations, taking into account the intensity relationship between Re K_α and K_β x rays. Evidence for the weak crossover transitions, 114.3 and 167.6 keV, is present in the data confirming the 44.1 and 70.0 keV lines as members of band E.

Bands F and G are strongly linked between them below the (11^+) levels which lie very close in both bands. Band G depopulates strongly into band F. The 139.1 keV is an unresolved doublet, one of its members has been placed in band G and the other one depopulates the same band G (not placed in the level scheme). Transitions of bands F and G and some of the connections between them are shown in Figs. 10(b) and 10(c).

Transition energies, spin assignments, γ-ray intensities, branching ratios, DCO ratios, and the evaluated $B(M1)/B(E2)$ are listed in Table II grouped in sequences for each band. γ-ray intensities were obtained from the total coincidence projection and from individual spectra in coincidence with low spin transitions and were normalized to the 99.5 keV line. The experimental branching ratio for a given state was obtained from relative γ-ray intensity in the spectrum in coincidence with transitions directly populating that state. For selected $\Delta I=1$ transitions, mixing ratios δ were estimated from angular correlation measurements. The DCO calculations have been carried out for $\theta_1=34.6°(145.4°)$, $\theta_2=90°$ and $\langle\phi\rangle=69.7°(\langle\phi\rangle)$ is the average relative angular position of the detectors at θ_1 and θ_2 in the GASP geometry). Values of δ were obtained for selected $\Delta I=1$ transitions of bands A, B, D, and E (Fig. 9) the calculations have been carried out using a width of $\sigma/I=0.3$ for the substate population distribution. The experimental $B(M1)/B(E2)$ ratios were determined by the following expression:

$$\frac{B(M1,I\rightarrow I-1)}{B(E2,I\rightarrow I-2)}=0.697\frac{E_{\gamma_2}^5}{E_{\gamma_1}^3}\frac{1}{\lambda(1+\delta^2)}\left[\frac{\mu_N^2}{(eb)^2}\right],$$

where E_{γ_1,γ_2} are the energies (in MeV) corresponding to the $\Delta I=1,2$ transitions, respectively, λ the γ-ray intensity ratio $I(\gamma_2)/I(\gamma_1)$, and δ is the mixing ratio of the $\Delta I=1$ transi-

TABLE II. γ-ray transition energies, spin assignments, γ intensities, branching ratios, DCO ratios and $B(M1)/B(E2)$ ratios in ^{176}Re.

E_λ (keV)[a]	$I_i^\pi \rightarrow I_f^\pi$	I_λ[b]	Branching ratio[c]	DCO ratio[d]	$B(M1)/B(E2)$[e] (μ_N^2/e^2b^2)
99.5	$(8^-)\rightarrow(7^+)$	1000		0.90(3)	
Band A					
70.5	$(9^-)\rightarrow(8^-)$				
122.4	$(10^-)\rightarrow(9^-)$	516		0.87(4)	
160.9	$(11^-)\rightarrow(10^-)$	761	0.14(3)	0.86(4)	2.1(5)
282.7	$(11^-)\rightarrow(9^-)$	99			
197.2	$(12^-)\rightarrow(11^-)$	627	0.28(5)	0.76(3)	1.9(3)
358.0	$(12^-)\rightarrow(10^-)$	221		0.99(7)	
222.6	$(13^-)\rightarrow(12^-)$	371	0.56(8)	0.87(4)	1.5(2)
419.7	$(13^-)\rightarrow(11^-)$	237		0.93(8)	
252.6	$(14^-)\rightarrow(13^-)$	354	0.64(9)	0.76(4)	1.6(2)
475.2	$(14^-)\rightarrow(12^-)$	235		0.97(5)	
274.3	$(15^-)\rightarrow(14^-)$	263	0.93(13)	0.81(5)	1.5(2)
526.7	$(15^-)\rightarrow(13^-)$	284		1.1(1)	
294.2	$(16^-)\rightarrow(15^-)$	192	1.2(2)	0.68(5)	1.3(2)
568.0	$(16^-)\rightarrow(14^-)$	250		0.98(4)	
313.4	$(17^-)\rightarrow(16^-)$	161	1.9(3)	0.64(5)	0.98(16)
607.5	$(17^-)\rightarrow(15^-)$	284		1.03(6)	
325.5	$(18^-)\rightarrow(17^-)$	95	3.0(5)	0.71(6)	0.71(12)
638.7	$(18^-)\rightarrow(16^-)$	262		1.02(5)	
342.8	$(19^-)\rightarrow(18^-)$	71	3.2(5)	0.72(6)	0.72(11)
668.3	$(19^-)\rightarrow(17^-)$	227		0.93(8)	
346.8	$(20^-)\rightarrow(19^-)$	77	2.6(4)	0.49(8)	1.00(15)
689.7	$(20^-)\rightarrow(18^-)$	181		1.06(5)	
363.5	$(21^-)\rightarrow(20^-)$	29	5(2)	0.75(8)	0.5(2)
710.2	$(21^-)\rightarrow(19^-)$	167		0.94(8)	
364.0	$(22^-)\rightarrow(21^-)$	19	8(3)		0.37(14)
727.5	$(22^-)\rightarrow(20^-)$	139		1.1(1)	
381.0	$(23^-)\rightarrow(22^-)$	19	3.7(8)		0.8(2)
745.8	$(23^-)\rightarrow(21^-)$	81			
387.5	$(24^-)\rightarrow(23^-)$	16	2.9(9)		1.1(3)
768.0	$(24^-)\rightarrow(22^-)$	53			
787.8	$(25^-)\rightarrow(23^-)$	71			
806.4	$(26^-)\rightarrow(24^-)$	28			
832.0	$(27^-)\rightarrow(25^-)$	34			
863	$(28^-)\rightarrow(26^-)$	15			
Band B					
37.5	$(6^-)\rightarrow(5^-)$				
56.2	$(7^-)\rightarrow(6^-)$				
62.7	$(8^-)\rightarrow(7^-)$		0.17(3)		0.39(7)
118.9	$(8^-)\rightarrow(6^-)$				
107.2	$(9^-)\rightarrow(8^-)$	127	0.32(5)	0.69(6)	0.25(4)
169.7	$(9^-)\rightarrow(7^-)$	42		0.87(15)	
93.3	$(10^-)\rightarrow(9^-)$	107	0.89(6)	0.7(1)	0.31(2)
200.2	$(10^-)\rightarrow(8^-)$	89		1.1(1)	
176.2	$(11^-)\rightarrow(10^-)$	282	0.71(5)	0.38(6)	0.25(2)
269.4	$(11^-)\rightarrow(9^-)$	210		0.92(7)	
124.3	$(12^-)\rightarrow(11^-)$	124	2.9(4)	0.50(6)	0.30(4)
300.4	$(12^-)\rightarrow(10^-)$	336		1.04(6)	
250.1	$(13^-)\rightarrow(12^-)$	168	1.3(2)	0.44(6)	0.25(4)
374.2	$(13^-)\rightarrow(11^-)$	255		1.0(4)	
158.8	$(14^-)\rightarrow(13^-)$	96	5.0(7)	0.49(6)	0.40(6)
408.8	$(14^-)\rightarrow(12^-)$	390		1.06(7)	
311.0	$(15^-)\rightarrow(14^-)$	81	1.9(3)	0.41(5)	0.28(4)
469.8	$(15^-)\rightarrow(13^-)$	176		0.96(5)	
200.8	$(16^-)\rightarrow(15^-)$	47	7.6(10)		0.39(5)
510.1	$(16^-)\rightarrow(14^-)$	422		1.02(6)	

TABLE II. (*Continued.*)

E_λ (keV)[a]	$I_i^\pi \rightarrow I_f^\pi$	I_λ[b]	Branching ratio[c]	DCO ratio[d]	$B(M1)/B(E2)$[e] (μ_N^2/e^2b^2)
359.5	$(17^-)\rightarrow(16^-)$	57	2.3(3)	0.40(6)	0.35(5)
558.4	$(17^-)\rightarrow(15^-)$	154		0.96(5)	
244.7	$(18^-)\rightarrow(17^-)$	19	8.0(20)	0.7(2)	0.47(12)
603.7	$(18^-)\rightarrow(16^-)$	193		1.0(1)	
391.3	$(19^-)\rightarrow(18^-)$	39	2.8(4)		0.43(6)
635.3	$(19^-)\rightarrow(17^-)$	116		1.01(6)	
296.9	$(20^-)\rightarrow(19^-)$	16	10(2)		0.41(8)
687.3	$(20^-)\rightarrow(18^-)$	146		1.04(6)	
407.8	$(21^-)\rightarrow(20^-)$				
703.7	$(21^-)\rightarrow(19^-)$	51		1.01(6)	
350.3	$(22^-)\rightarrow(21^-)$				
760.9	$(22^-)\rightarrow(20^-)$	109		0.97(7)	
763.3	$(23^-)\rightarrow(21^-)$			0.95(8)	
823.0	$(24^-)\rightarrow(22^-)$				
820.5	$(25^-)\rightarrow(23^-)$				
870.4	$(26^-)\rightarrow(24^-)$				
868	$(27^-)\rightarrow(25^-)$				
899	$(28^-)\rightarrow(26^-)$				
Transitions	from A to B				
307.9	$(12^-)\rightarrow(10^-)$	46			
354.4	$(13^-)\rightarrow(11^-)$	39			
230	$(13^-)\rightarrow(12^-)$	13		0.9(2)	
483.2	$(14^-)\rightarrow(12^-)$	11			
232	$(14^-)\rightarrow(13^-)$	3			
346.2	$(15^-)\rightarrow(14^-)$	3			
Transitions	from B to A				
350.2	$(12^-)\rightarrow(10^-)$	39		1.00(7)	
189.5	$(12^-)\rightarrow(11^-)$	187		0.78(6)	
401.4	$(14^-)\rightarrow(12^-)$	70		1.1(1)	
179.4	$(14^-)\rightarrow(13^-)$	17		0.87(7)	
490.3	$(15^-)\rightarrow(13^-)$	49			
Band C					
437.4	(12,14)→(10,12)	101			
201.3	(13,15)→(12,14)	79		0.9(2)	
234.9	(14,16)→(13,15)	85	0.26(6)	0.9(2)	3.3(8)
437.1	(14,16)→(12,14)	22			
263.1	(15,17)→(14,16)	67	0.41(10)		2.9(7)
498.3	(15,17)→(13,15)	27			
287.8	(16,18)→(15,17)	28	0.8(2)		1.9(5)
551.8	(16,18)→(14,16)	23			
309.3	(17,19)→(16,18)	18	2.0(6)		0.9(3)
597.2	(17,19)→(15,17)	35			
327.8	(18,20)→(17,19)	26	0.8(2)		2.6(6)
636.7	(18,20)→(16,18)	22			
339.8	(19,21)→(18,20)	17	1.2(3)		1.9(5)
667.4	(19,21)→(17,19)	20			
370.3	(20,22)→(19,21)	8	1.1(3)		2.2(6)
710.4	(20,22)→(18,20)	9			
Transitions	from C to A				
946.7	$(10,12)\rightarrow(10^-)$	116		1.1(1)	
786.2	$(10,12)\rightarrow(11^-)$	125		0.48(8)	
1026.4	$(12,14)\rightarrow(12^-)$			1.0(1)	
803.8	$(12,14)\rightarrow(13^-)$	81		0.5(1)	

TABLE II. (*Continued.*)

E_λ (keV)[a]	$I_i^\pi \rightarrow I_f^\pi$	I_λ[b]	Branching ratio[c]	DCO ratio[d]	$B(M1)/B(E2)$[e] (μ_N^2/e^2b^2)
Band D	favored sequence				
76.2	$5^+ \rightarrow 3^+$	58		1.1(1)	
171.3	$7^+ \rightarrow 5^+$	347		1.03(3)	
267.8	$9^+ \rightarrow 7^+$	500		0.97(5)	
359.3	$11^+ \rightarrow 9^+$	469		0.96(4)	
441.3	$13^+ \rightarrow 11^+$	442		0.93(5)	
509.8	$15^+ \rightarrow 13^+$	414		0.98(3)	
553.0	$17^+ \rightarrow 15^+$	303		1.01(4)	
565.8	$19^+ \rightarrow 17^+$	217		1.11(7)	
600.8	$21^+ \rightarrow 19^+$	186		0.9(1)	
661.6	$23^+ \rightarrow 21^+$	94		1.1(1)	
725.2	$25^+ \rightarrow 23^+$	62		1.0(1)	
783.7	$27^+ \rightarrow 25^+$	22			
840.1	$29^+ \rightarrow 27^+$	12			
Band D	unfavored sequence				
162.4	$6^+ \rightarrow 4^+$	105		1.17(13)	
258.3	$8^+ \rightarrow 6^+$	177		0.97(17)	
349.3	$10^+ \rightarrow 8^+$	146		0.98(13)	
431.0	$12^+ \rightarrow 10^+$	126		0.96(16)	
500.5	$14^+ \rightarrow 12^+$	119		1.2(2)	
533.2	$16^+ \rightarrow 14^+$	118		1.1(2)	
Transitions	from the unfavored	into the	favored	sequence	of band D
141.3	$4^+ \rightarrow 3^+$	13			
65.0	$4^+ \rightarrow 5^+$	17			
227.3	$6^+ \rightarrow 5^+$	20		0.73(10)	
56.0	$6^+ \rightarrow 7^+$				
314.3	$8^+ \rightarrow 7^+$	11			
46.5	$8^+ \rightarrow 9^+$				
396.0	$10^+ \rightarrow 9^+$	7			
467.6	$12^+ \rightarrow 11^+$	6			
Band E					
44.1	$I_0+1 \rightarrow I_0$				
70.0	$I_0+2 \rightarrow I_0+1$		0.05(2)		0.8(3)
114.3	$I_0+2 \rightarrow I_0$				
97.4	$I_0+3 \rightarrow I_0+2$	27	0.19(5)	0.71(10)	0.52(14)
167.6	$I_0+3 \rightarrow I_0+1$				
122.0	$I_0+4 \rightarrow I_0+3$	55	0.66(13)	0.73(10)	0.29(6)
219.3	$I_0+4 \rightarrow I_0+2$	29		1.0(1)	
149.1	$I_0+5 \rightarrow I_0+4$	91	0.83(12)	0.51(5)	0.37(5)
270.7	$I_0+5 \rightarrow I_0+3$	76		1.2(2)	
171.7	$I_0+6 \rightarrow I_0+5$	64	1.3(3)	0.48(5)	0.36(8)
320.3	$I_0+6 \rightarrow I_0+4$	110		0.97(5)	
197.2	$I_0+7 \rightarrow I_0+6$	63	1.8(3)	0.6(1)	0.34(6)
368.7	$I_0+7 \rightarrow I_0+5$	136		1.03(7)	
217.3	$I_0+8 \rightarrow I_0+7$	40	2.9(6)	0.43(6)	0.28(6)
414.3	$I_0+8 \rightarrow I_0+6$	137		1.1(1)	
240.2	$I_0+9 \rightarrow I_0+8$	47	2.5(5)	0.49(7)	0.40(8)
457.2	$I_0+9 \rightarrow I_0+7$	118		1.0(1)	
257.3	$I_0+10 \rightarrow I_0+9$	19	4.3(11)	0.54(6)	0.29(7)
497.3	$I_0+10 \rightarrow I_0+8$	138		1.0(1)	
275	$I_0+11 \rightarrow I_0+10$	20	6.1(15)	0.5(1)	0.23(6)
532.4	$I_0+11 \rightarrow I_0+9$	117		1.1(1)	
291	$I_0+12 \rightarrow I_0+11$	21	4.8(11)		0.34(8)
566.0	$I_0+12 \rightarrow I_0+10$	103		0.97(7)	
291	$I_0+13 \rightarrow I_0+12$	10	6.6(13)		0.29(6)
582.2	$I_0+13 \rightarrow I_0+11$	65		0.9(1)	

TABLE II. (*Continued.*)

E_λ (keV)[a]	$I_i^\pi \rightarrow I_f^\pi$	I_λ[b]	Branching ratio[c]	DCO ratio[d]	$B(M1)/B(E2)$[e] (μ_N^2/e^2b^2)
Band F					
179.7	$(8^+)\rightarrow(7^+)$	179		0.75(7)	
200.0	$(9^+)\rightarrow(8^+)$	87	0.41(4)	0.9(1)	1.7(2)
379.7	$(9^+)\rightarrow(7^+)$	35		1.1(1)	
226.9	$(10^+)\rightarrow(9^+)$	43	0.85(7)	0.71(8)	1.0(1)
427.1	$(10^+)\rightarrow(8^+)$	36		0.88(9)	
231.5	$(11^+)\rightarrow(10^+)$	53	1.1(1)		1.0(1)
458.8	$(11^+)\rightarrow(9^+)$	54		0.9(1)	
247.9	$(12^+)\rightarrow(11^+)$	23	1.0(1)	0.8(2)	1.2(1)
479.9	$(12^+)\rightarrow(10^+)$	23		1.1(2)	
259.4	$(13^+)\rightarrow(12^+)$	19	1.6(2)	0.9(1)	0.84(11)
507.7	$(13^+)\rightarrow(11^+)$	34		0.9(2)	
269.8	$(14^+)\rightarrow(13^+)$	21	1.5(2)		0.98(13)
529.6	$(14^+)\rightarrow(12^+)$	29		1.1(1)	
277.3	$(15^+)\rightarrow(14^+)$	15	1.9(3)		0.84(13)
547.5	$(15^+)\rightarrow(13^+)$	29		0.9(1)	
560.8	$(16^+)\rightarrow(14^+)$	29			
604.0	$(17^+)\rightarrow(15^+)$				
571.6	$(18^+)\rightarrow(16^+)$	11			
Band G					
91.9	$(8^+)\rightarrow(7^+)$				
139.1	$(9^+)\rightarrow(8^+)$		0.41(6)	0.78(6)	0.42(6)
231.9	$(9^+)\rightarrow(7^+)$				
162.6	$(10^+)\rightarrow(9^+)$	21	0.82(7)	0.53(8)	0.49(4)
301.5	$(10^+)\rightarrow(8^+)$	22		0.9(1)	
201.3	$(11^+)\rightarrow(10^+)$	110	0.50(7)		1.08(15)
363.5	$(11^+)\rightarrow(9^+)$	41		0.9(1)	
224.2	$(12^+)\rightarrow(11^+)$	37	1.3(2)	0.9(1)	0.66(10)
425.6	$(12^+)\rightarrow(10^+)$	49		0.97(5)	
240.6	$(13^+)\rightarrow(12^+)$	23	3.0(6)	0.9(1)	0.36(7)
465.7	$(13^+)\rightarrow(11^+)$	58		1.07(6)	
262.7	$(14^+)\rightarrow(13^+)$	16	2.7(5)	0.82(6)	0.46(9)
504.1	$(14^+)\rightarrow(12^+)$	41		1.07(7)	
270.6	$(15^+)\rightarrow(14^+)$	8	7.9(23)	0.84(7)	0.19(6)
533.2	$(15^+)\rightarrow(13^+)$	52		0.99(6)	
286.0	$(16^+)\rightarrow(15^+)$	5	9(3)		0.18(6)
556.2	$(16^+)\rightarrow(14^+)$	47		1.06(6)	
291.0	$(17^+)\rightarrow(16^+)$	4	6(3)		0.30(15)
577.3	$(17^+)\rightarrow(15^+)$	26		1.2(2)	
599.2	$(18^+)\rightarrow(16^+)$	23			
617.5	$(19^+)\rightarrow(17^+)$				
631.2	$(20^+)\rightarrow(18^+)$				
658.1	$(21^+)\rightarrow(19^+)$				
Transitions	from F to G				
181.5	$(10^+)\rightarrow(9^+)$	8			
250.9	$(11^+)\rightarrow(10^+)$	23			
Transitions	from G to F				
193.9	$(7^+)\rightarrow(7^+)$			0.8(2)	
407.6	$(10^+)\rightarrow(8^+)$	32		1.1(1)	
207.9	$(10^+)\rightarrow(9^+)$	53		0.9(1)	
409.1	$(11^+)\rightarrow(9^+)$	15			

[a]Uncertainties between 0.1 and 0.3 keV.

[b]Uncertainties between 5 and 30 %.

[c]Branching ratio: $I\gamma(I\rightarrow I-2)/I\gamma(I\rightarrow I-1)$, $I\gamma(I\rightarrow I-2)$ and $I\gamma(I\rightarrow I-1)$ are the relative γ intensities of the $\Delta I=2$ and $\Delta I=1$ transitions depopulating the spin I level, respectively.

[d]Directional correlation ratio: $I\gamma_{\text{gate}=\theta_2}(\theta_1)/I\gamma_{\text{gate}=\theta_1}(\theta_2)$, ($\theta_1$ = 31.7°, 36°, 144°, and 148.3° and θ_2 = 90°) determined from coincidence spectra, setting gates on stretched $E2$ transitions on both axes of the DCO matrix.

[e]Determined assuming $\delta^2=0$.

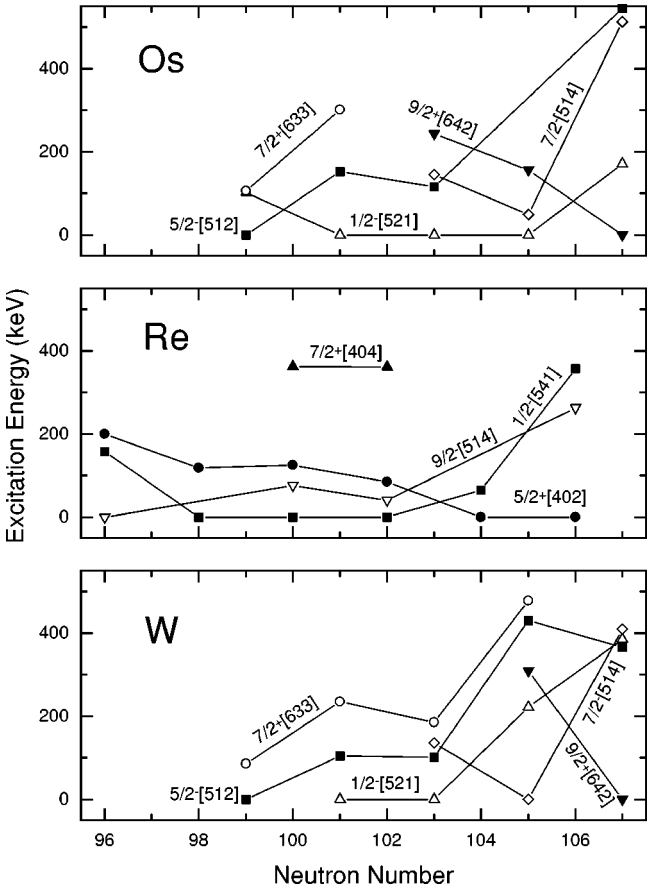

FIG. 11. Bandhead excitation energies for odd Os, Re, and W isotopes. The energy for the $\pi 1/2^-[541]$ orbital in ^{171}Re corresponds to the calculated value reported in Ref. [21].

tion. For the $B(M1)/B(E2)$ reported in Table II we assumed $\delta^2=0$ (for $|\delta|<0.3$ the errors produced with this assumption are less than 10%).

III. DISCUSSION

The identification of proton and neutron orbitals involved in the rotational bands of ^{176}Re was done on the basis of the coupling schemes proposed in Refs. [2,3,20]. The evolution of Nilsson levels in the vicinity of ^{176}Re as a function of the neutron number is shown in Fig. 11, where the bandhead energies have been plotted for the odd Os, Re, and W isotopes [15,17,18,21–27]. For the doubly odd ^{176}Re we constructed the zero-order level scheme adding the experimental bandhead energies extracted from neighboring odd proton and odd neutron isotopes and neglecting the residual interaction which can split the $K_\pm=|\Omega_p\pm\Omega_n|$ states according to the Gallagher-Moszkowski coupling rules [28] (see Table III). For the ^{176}Re rotational bands found in the present work, the configuration assignment was based as said, on the classification of coupling schemes [2,3,20], on systematics and on the analysis of band properties such as rotation alignments, band crossing frequencies, $B(M1)/B(E2)$ values, mixing ratios of $M1(E2)$ transitions, signature splitting, etc. The theoretical estimates of the $B(M1)/B(E2)$ were obtained from the semiclassical formula of the cranking model developed by Dönau and Frauendorf [29] (see also Ref. [30]). We used the following expressions:

TABLE III. Zero-order level scheme of ^{176}Re. Entries are $K_\pm=|\Omega_p\pm\Omega_n|$ values and zero-order energies in keV. Excitation energies correspond to the average of ^{175}Re and ^{177}Re for protons and to the average of ^{175}W and ^{177}Os for neutrons. (The values corresponding to proton and neutron intrinsic spins aligned have been underlined.)

$\pi\Omega_p^\pi[Nn_3\Lambda]$	$\nu\Omega_n^\pi[Nn_3\Lambda]$	$\nu 1/2^-[521]$	$\nu 5/2^-[512]$	$\nu 7/2^+[633]$
E_π(keV)	E_ν(keV)	0	128	268
$\pi 1/2^-[541]$		$0^+,1^+$	$2^+,3^+$	$3^-,4^-$
0		$\underline{0}^-$	$\underline{128}$	$\underline{268}$
$\pi 9/2^-[514]$		$4^+,5^+$	$2^+,7^+$	$1^-,8^-$
58		$\underline{58}$	$18\overline{6}$	$32\overline{6}$
$\pi 5/2^+[402]$		$2^-,3^-$	$0^-,5^-$	$1^+,6^+$
105		$\underline{105}$	$23\overline{3}$	$37\overline{5}$
$\pi 7/2^+[404]$		$3^-,4^-$	$1^-,6^-$	$0^+,7^+$
361		$36\overline{1}$	$\underline{489}$	$\underline{629}$

$$B(E2,I\rightarrow I-2)=\frac{5}{16\pi}\langle IK20|I-2K\rangle^2 Q_0^2$$

and

$$B(M1,I\rightarrow I-1)=\frac{3}{8\pi}\mu_T^2,$$

where μ_T is the transverse magnetic moment given by

$$\mu_T=(g_{\Omega_p}-g_R)(\Omega_p\sqrt{1-K^2/I^2}-i_pK/I)+(g_{\Omega_n}-g_R)\times(\Omega_n\sqrt{1-K^2/I^2}-i_nK/I),$$

in units of μ_N. Q_0 is the intrinsic quadrupole moment, g_{Ω_p}, g_{Ω_n}, and $g_R=0.3$ are the proton, neutron, and collective gyromagnetic factors, respectively. The quantities i_p and i_n represent the aligned angular momenta of the proton and the neutron, respectively.

The mixing ratio δ for $\Delta I=1$ in-band transitions was evaluated using the expression: $\delta=0.93E_\gamma Q_0K\sqrt{I^2-K^2}/(\mu_T I^2)$, where E_γ is the transition energy in MeV, Q_0, and μ_T are in units of eb and μ_N, respectively. Q_0 was taken as 6.4 e b, a characteristic value in this region. [For example, the value for the transition quadrupole moment of the 2^+ state of ^{174}W extracted from the experimental lifetime [31] is 6.3(2) e b.] For each $\Delta I=2$ rotational band the inertia parameters, J_0 and J_1 were extracted fitting the level energies through a fourth-order cranking formula:

$$E=\tfrac{1}{2}(J_0+\tfrac{3}{2}J_1\omega^2)\omega^2,$$

where the rotational frequencies ω are obtained from the third-order equation:

$$R=I_x-i=\sqrt{(I+\tfrac{1}{2})^2-K^2}-i=(J_0+J_1\omega^2)\omega,$$

TABLE IV. Moments of inertia, alignments, calculated alignments ($i^{\rm calc}=i_n+i_p$), band-crossing frequencies, experimental and calculated deviations of the crossing frequencies with respect to the even-even core (gsb, ground state band of ^{174}W). The calculated deviations $\delta\hbar\omega_c^{\rm calc}$ are obtained adding the deviations of the odd-N and odd-Z neighboring nuclei.

Nucleus	Band	α	$J_0/\hbar^2$ (MeV^{-1})	$J_1/\hbar^4$ (MeV^{-3})	i ($\hbar$)	$i^{\rm calc}$ ($\hbar$)	$\hbar\omega_c$ (MeV)	$\delta\hbar\omega_c$ (MeV)	$\delta\hbar\omega_c^{\rm calc}$ (MeV)
^{174}W	gsb	0	25.8	187.0	0		0.300		
^{175}W	$7/2^+[633]$	1/2	38.3	38.1	2.80		>0.34	>0.04	
^{175}W	$7/2^+[633]$	$-1/2$	32.7	67.0	2.87		>0.34	>0.04	
^{175}W	$1/2^-[521]$	1/2	35.0	169.1	0.42		0.257	-0.043	
^{175}W	$1/2^-[521]$	$-1/2$	34.8	163.3	-0.35				
^{175}W	$5/2^-[512]$	1/2	34.4	141.8	0.20				
^{175}W	$5/2^-[512]$	$-1/2$	31.9	169.3	0.46				
^{177}W	$7/2^+[633]$	1/2	39.0	46.7	2.52		0.368	0.068	
^{177}W	$7/2^+[633]$	$-1/2$	33.9	54.3	2.77		0.368	0.068	
^{175}Re	$9/2^-[514]$	1/2	15.7	379.4	1.41		0.263	-0.037	
^{175}Re	$9/2^-[514]$	$-1/2$	3.54	476.4	2.99				
^{175}Re	$1/2^-[541]$	1/2	32.3	45.7	2.76		0.315	0.015	
^{175}Re	$5/2^+[402]$	1/2	25.8	405.9	0.16				
^{175}Re	$5/2^+[402]$	$-1/2$	34.2	301.4	-0.70				
^{175}Re	$7/2^+[404]$	1/2	36.8	181.5	-0.27				
^{175}Re	$7/2^+[404]$	$-1/2$	33.5	235.4	0.02				
^{176}Re	A	0	33.9	97.4	3.67	4.28	0.335	0.035	0.031
^{176}Re	A	1	27.0	141.8	4.62	4.21	0.335	0.035	0.031
^{176}Re	B	0	33.9	42.8	6.02	5.63	≈ 0.4	≈ 0.1	0.083
^{176}Re	B	1	36.3	51.5	5.18	5.56	≈ 0.4	≈ 0.1	0.083
^{176}Re	D	0	38.6	84.7	2.32	2.41			
^{176}Re	D	1	38.2	82.4	3.18	3.18	0.280	-0.020	-0.028

where R is the collective and i is the particle contribution (which is also set as a free parameter in the calculation) to the total aligned angular momentum I_x. Table IV summarizes the results obtained using this procedure for the inertia parameters J_0 and J_1 together with the extracted alignments and crossing frequencies for bands A, B, and D of ^{176}Re and for structures of interest in the odd neighbors ^{175}Re [15] and ^{175,177}W [15,22] and the even-even core ^{174}W [31]. Proton and neutron g factors ($g_{\Omega_p}, g_{\Omega_n}$) were calculated by the expression [32]: $g_\Omega = g_l + (g_s - g_l)\langle s_3\rangle/\Omega$. The expectation values of the spin projection on the symmetry axis, $\langle s_3\rangle$, were evaluated using Nilsson-type wave functions obtained from the diagonalization of the deformed harmonic oscillator with $\beta=0.24$, the parameters κ and μ were extracted from Ref. [32]. For the orbital and spin g factors we used: $g_{l,p}=1$; $g_{s,p}=3.91$; $g_{l,n}=0$; and $g_{s,n}=-2.68$. Alignments, $\langle s_3\rangle$ and g factors for the proton and neutron intrinsic states used in the calculations are listed in Table V.

A. Band A

Band A is described by the configuration $\pi h_{11/2}(9/2^-[514])\otimes\nu i_{13/2}(7/2^+[633])$. This structure corresponds to the yrast band in most nuclei of the light rare-earth region (Eu, Tb, Ho, Tm, and Lu [33–37]) . In all these bands the phenomenon of signature inversion has systematically been observed in the neighborhood of $A\approx 160$. At high spins, namely above the signature inversion point, states with even spin ($\alpha=0$) are favored, corresponding to the coupling between the favored signatures in both proton ($\alpha^f=-1/2$) and neutron ($\alpha^f=+1/2$) orbitals, while the signature splitting is anomalous in the low-spin regime. The signature inversion

TABLE V. Parameters used in the calculations of $B(M1)$ values. The alignments were extracted from ^{175}Re and ^{175}W for the proton and neutron orbitals, respectively. The expectation values $\langle s_3\rangle$ were calculated using Nilsson wave functions (see text).

	Protons				Neutrons		
Orbital	$i(\hbar)$	$\langle s_3\rangle$	g_Ω	Orbital	$i(\hbar)$	$\langle s_3\rangle$	g_Ω
$\pi 9/2^-[514]$	1.41	0.45	1.29	$\nu 7/2^+[633]$	2.80	0.33	-0.25
$\pi 1/2^-[541]$	2.76	-0.03	0.84	$\nu 1/2^-[521]$	0.42	-0.13	0.71
$\pi 5/2^+[402]$	0.16	0.49	1.57	$\nu 5/2^-[512]$	0.46	0.29	-0.31
$\pi 7/2^+[404]$	0.02	-0.44	0.63				

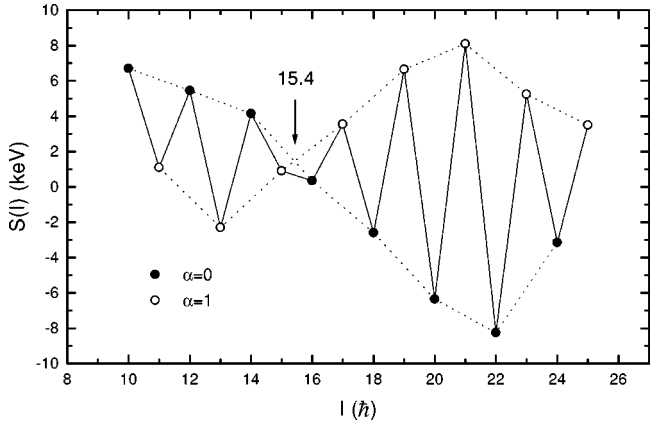

FIG. 12. Variation of the energy difference $S(I)=E(I)-E(I-1)-[E(I+1)-E(I)+E(I-1)-E(I-2)]/2$ between levels of the $\pi h_{11/2}\otimes\nu i_{13/2}$ structure of ^{176}Re (band A) as a function of the angular momentum. The signature inversion is observed at $15.4\hbar$.

can be seen in a plot of $E(I)-E(I-1)$ vs I, where $E(I)$ denotes the excitation energy of the level with spin $I\hbar$. If the signature splitting is small, the quantity $S(I)=E(I)-E(I-1)-[E(I+1)-E(I)+E(I-1)-E(I-2)]/2$ has a higher sensitivity than $E(I)-E(I-1)$ [35,38]. Such a plot of $S(I)$ vs I for band A of ^{176}Re is shown in Fig. 12, the arrow indicates the inversion point. For the adopted spin values for band A, favored states correspond to the $\alpha=1(0)$ signature at low (high) spins, as it is expected for the $\pi h_{11/2}\otimes\nu i_{13/2}$ structure. The behavior of the signature inversion for different chains of isotopes and isotones has been recently analyzed [39–41] and general trends have been found for nuclei with $Z=63-73$, $N=89-95$. Here we present a systematic study extended with the new experimental data available and plot the inversion point vs $N-Z$ (Fig. 13). The data for the $\pi h_{11/2}\otimes\nu i_{13/2}$ band in ^{178}Re [51] are also included, spins have been changed adding one unit to the values assigned in Ref. [51] to conform with the systematics of the staggering phase. The inversion point remains fairly constant for nuclei with the same value of $N-Z$ and decreases when $N-Z$ increases. The phenomenon of anomalous signature splitting and the inversion observed in the $\pi h_{11/2}\otimes\nu i_{13/2}$ structures has been extensively studied through a variety of theoretical approaches. In the framework of the cranking shell model, Bengtsson *et al.* [52] interpreted the signature inversion as a consequence of a triaxial deformation. The two-quasiparticle- plus-rotor model was also used to investigate this phenomenon. Hamamoto [53] applied this model to the $\pi h_{11/2}\otimes\nu i_{13/2}$ structure of ^{156}Tb and showed that the anomalous signature splitting at low spins is consistent with an axially symmetric shape (without residual proton-neutron interaction). Semmes and Ragnarsson [54] included in the particle-plus-rotor model a zero-range residual proton-neutron interaction with a spin-spin component and employed it to study the $\pi h_{11/2}\otimes\nu i_{13/2}$ band of ^{152}Eu, the application reproduced successfully the angular momentum at which the signature inversion occurs. Other explanations have been attempted using the angular-momentum projection method [55] and the interacting boson-fermion model [56]. In spite of these efforts, the essential mechanism for the signature inversion in the $\pi h_{11/2}\otimes\nu i_{13/2}$ bands is still an open question.

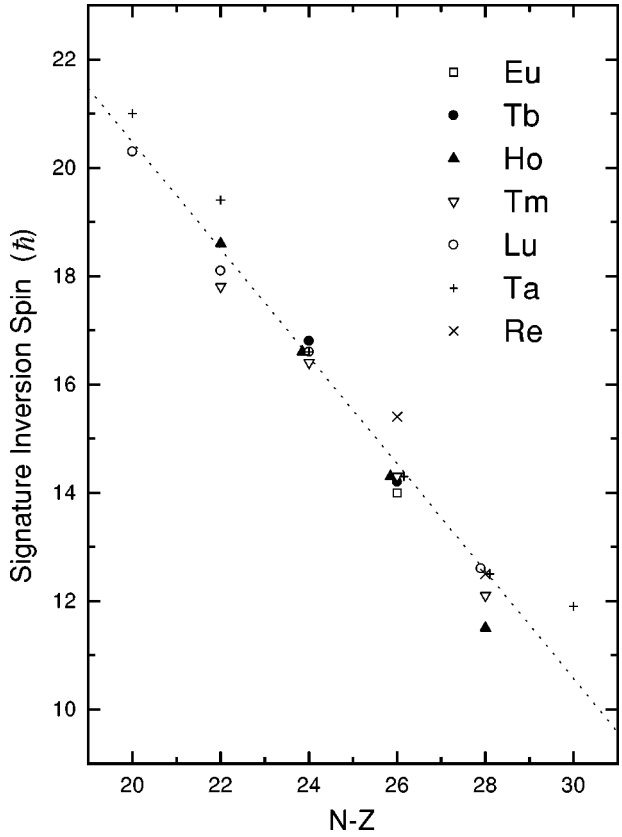

FIG. 13. Systematics of the inversion point in the $\pi h_{11/2}\otimes\nu i_{13/2}$ structure of nuclei with $Z=63-75$ (Eu, Tb, Ho, Tm, Lu, Ta and Re) and $N=89-103$. The data sources are: ^{152}Eu [33], ^{154,156}Tb [34], ^{156}Ho [42], ^{158}Ho [43], ^{160}Ho [35,40], ^{162}Ho [44], ^{160,162,164,166}Tm [36], ^{162,164,166}Lu [37,39,30], ^{170}Lu [45], ^{166}Ta [46], ^{168}Ta [47], ^{170}Ta [48], ^{172}Ta [49], ^{174}Ta [8,9], ^{176}Ta [50], ^{176}Re (this work), and ^{178}Re [51]. For ^{156}Tb, ^{158}Ho, and ^{168}Ta the new spin assignments proposed in Ref. [41] have been adopted. The dotted line represents a linear fit through the data points.

The alignment of band A shown in Fig. 14(a) follows the additivity rule in a large range of frequencies (Table IV) and exhibits a gain at a relatively high frequency (with respect to the even-even core). The crossing frequency was extracted from the Routhian [Fig. 14(b)], and is consistent with the breaking of a pair of $i_{13/2}$ neutrons in the presence of the $\pi h_{11/2}$ and the $\nu i_{13/2}$ orbitals. The $\nu i_{13/2}$ produces a delay in the crossing frequency most likely due to blocking, while the $\pi h_{11/2}$ reduces the crossing frequency with respect to the even-even core. This shift of the crossing to lower frequency in the $\pi h_{11/2}$ bands have been understood in terms of small β and negative-γ driving effects of this configuration [57], thus enhancing the action of the Coriolis force on the pair of $i_{13/2}$ neutrons. The shift in the crossing frequency in band A is in very good agreement with the sum of the shifts in the odd neutron (^{177}W) and odd proton (^{175}Re) neighboring nuclei (Table IV).

As mentioned before, the 99.5 keV transition which depopulates band A has a $B(E1,99.5\ \text{keV})=5.3(5)\times10^{-6}$ W.u. corresponding to a hindrance factor with respect to the Weisskopt estimate of $F_W^{E1}\approx2\times10^5$. This value falls within the systematics [58] for a $\Delta K=0$ or 1 transition. $E1$ transitions have been reported in the neighboring odd neutron nuclei (^{175,177}W [59,22] and ^{177}Os [60]) connecting

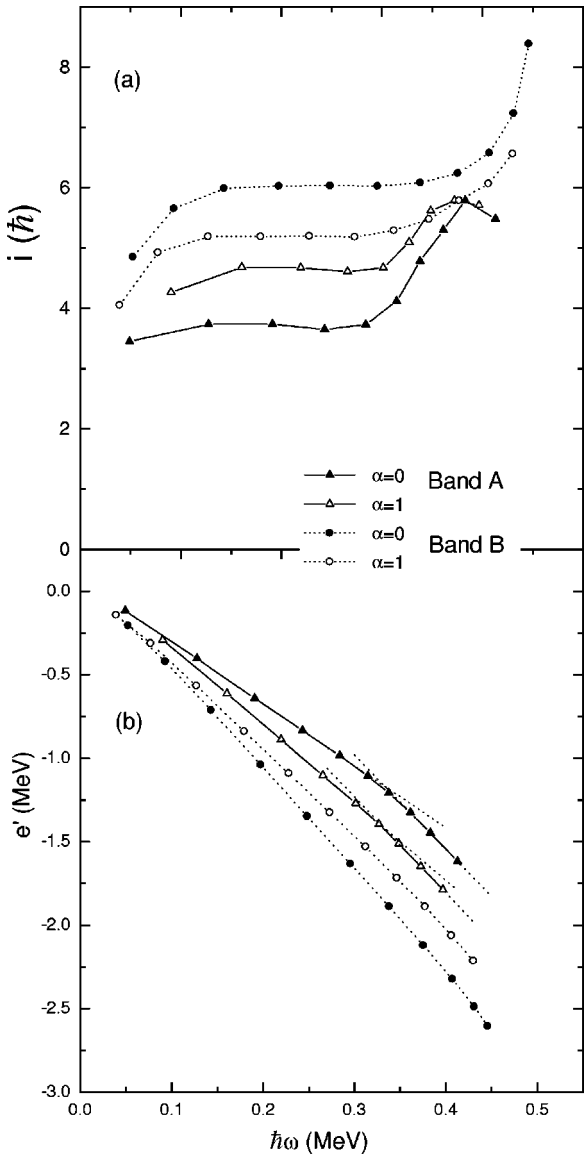

FIG. 14. Experimental alignments (a) and Routhians (b) as a function of the rotational frequency for bands A and B of ^{176}Re. The inertia parameters used for the reference configurations are reported in Table IV.

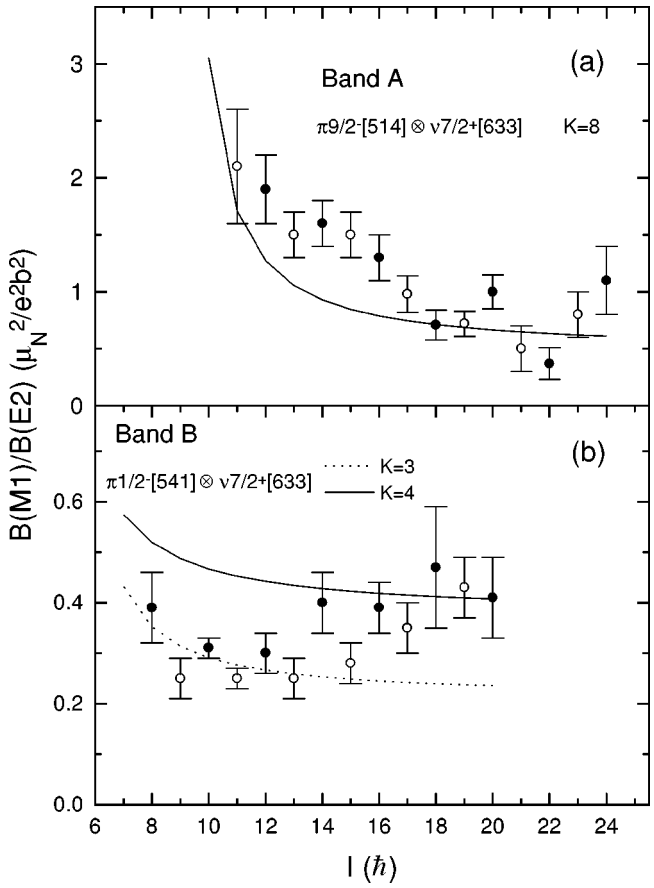

FIG. 15. Experimental $B(M1)/B(E2)$ values corresponding to bands A (a) and B (b) of ^{176}Re. The results of the calculations obtained in the framework of the cranking model for the configurations assigned to bands A and B are also shown. Solid and open circles correspond to the $\alpha=0$ and $\alpha=1$ signature, respectively.

the $7/2^+$ of the $i_{13/2}$ structure with the $5/2^-$ and the $7/2^-$ levels of the $5/2^-[512]$ band having $B(E1)$ in the range $0.12-15\times10^{-6}$ W.u. Based on these observations the decay of band A through the 99.5 $E1$ transition has been interpreted as a change of the neutron configuration from the $7/2^+[633]$ to the $5/2^-[512]$ orbital. This is indicated in the level scheme (Fig. 2), where we tentatively placed the 99.5 keV feeding the band head of band F having an assigned configuration of $\pi 9/2^-[514]\otimes\nu 5/2^-[512]$ (see the discussion of band F below).

The in-band decay properties are consistent with the configuration assignment. For example the measured $B(M1)/B(E2)$ are in good agreement with the calculated ones for the $\pi 9/2^-[514]\otimes\nu 7/2^+[633]$ configuration [Fig. 15(a)]. Furthermore the DCO ratios for the $\Delta I=1$ transitions in band A, which are around $0.7-0.9$ imply positive sign for δ. As an example a mixing ratio, $\delta=0.31(3)$ was estimated for the $(11^-)\rightarrow(10^-)$ 160.9 keV transition (Fig. 9). This is in agreement with the predictions obtained using the expression for δ indicated in the previous section of $\delta\approx+0.3$.

B. Band B

The configuration proposed for band B is the $\pi h_{9/2}(1/2^-[541])\otimes\nu i_{13/2}(7/2^+[633])$, where the orbitals in parenthesis should be the largest components of the intervening $\pi h_{9/2}$ and the $\nu i_{13/2}$ multiplets. Similar bands have been observed in a number of doubly odd Tm [8], Lu [45], Ta [9,50,61,62], Re [51], Ir [4,5], and Tl [1,63] isotopes and have been characterized as semidecoupled structures [1,4]. The large alignment is consistent with the involvement of the $\pi h_{9/2}$ and the $\nu i_{13/2}$ orbitals, in Table IV the alignment is shown in comparison with that predicted by the additivity rule [4]. The inertia parameters J_0, J_1 have been extracted using $K=3.5$. Figure 14(a) shows the alignment vs frequency, the $\alpha=0$ signature has an alignment $i\approx6\hbar$ and it begins to upbend at considerably higher frequency ($\hbar\omega\approx0.4$ MeV) than the ground-state band of the even-even core, as well as the other bands in the odd W, Re, and doubly odd ^{176}Re (Table IV). Such a delayed backbend is due to the added effects of the $\pi h_{9/2}$ and the $\nu i_{13/2}$ [64]. In Fig. 14(b) the Routhian of band B is plotted vs the rotational frequency. The configuration assignment is also supported by the agreement between measured and calculated $B(M1)/B(E2)$ val-

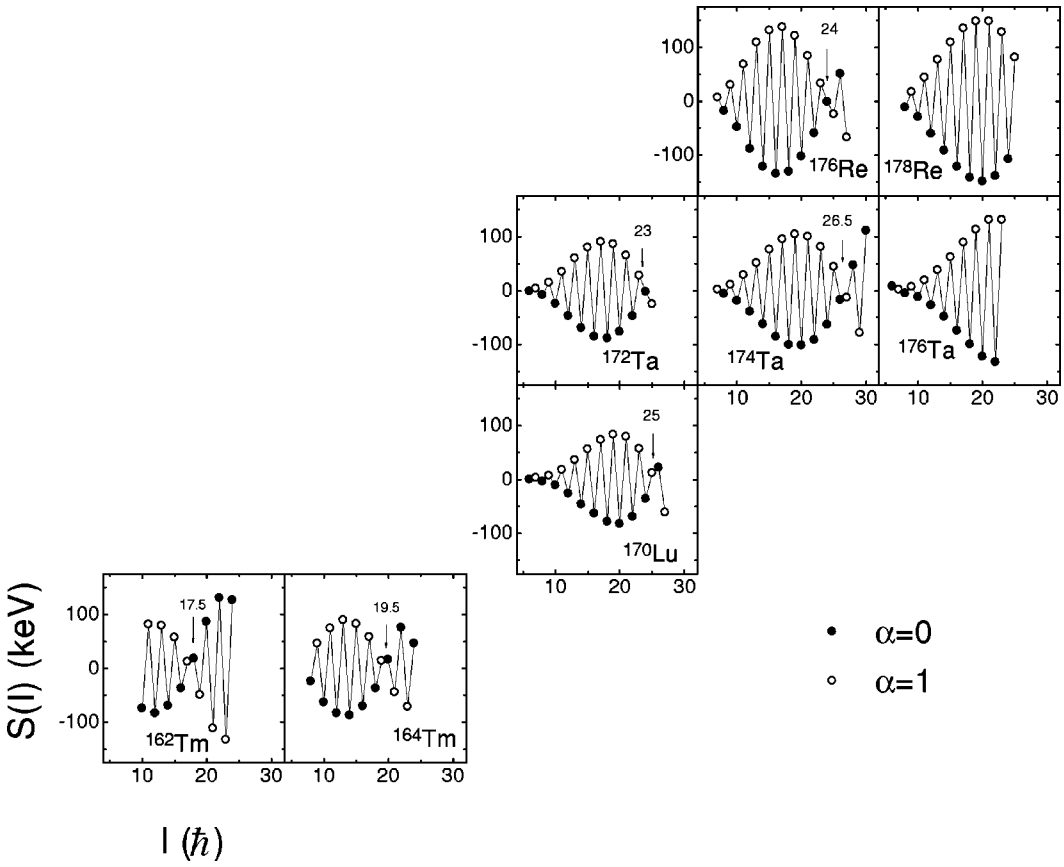

FIG. 16. Systematics of the signature splitting $S(I)=E(I)-E(I-1)-[E(I+1)-E(I)+E(I-1)-E(I-2)]/2$ vs I of the $\pi h_{9/2}\otimes\nu i_{13/2}$ bands in doubly odd nuclei: ^{162,164}Tm [8], ^{170}Lu [45], ^{172}Ta [49], ^{174}Ta [8], ^{176}Ta [50], ^{176}Re (this work), and ^{178}Re [51]. The arrows point at the signature inversion.

ues for this configuration, with the two values of $K=3$ and $K=4$ [Fig. 15(b)]. The experimental DCO ratios for the $\Delta I=1$ in-band transitions correspond to negative mixing ratios, which are well reproduced using the expression for δ given previously. For example, a value of $\delta=-0.17(10)$ was extracted for the $(14^-)\rightarrow(13^-)158.8$ keV transition of band B (Fig. 9) vs $\delta=-0.09$ and $\delta=-0.16$ calculated using $K=3$ and $K=4$, respectively. Another special feature of this structure is that it shows a pronounced level staggering. In Fig. 16 the signature splitting $S(I)$ (as defined in the previous section) is plotted vs angular momentum I for the $\pi h_{9/2}\otimes\nu i_{13/2}$ structures identified in ^{162,164}Tm [8], ^{170}Lu [45], ^{172}Ta [49], ^{174}Ta [8,9], ^{176}Ta [50], ^{176}Re (this work), and ^{178}Re [51]. Spins in ^{178}Re have been changed in one unit, consistent with the change performed in the $\pi h_{11/2}\otimes\nu i_{13/2}$ band and in line with the determination made in Ref. [9]. As can be seen in Fig. 16 favored states have even spins ($\alpha=0$) up to high-spin values where a change of phase is produced. This is contrary to the expected favored signature in the odd-odd nucleus (α^f_{p-n}) corresponding to the coupling between the favored signature of both proton (α^f_p) and neutron (α^f_n) orbitals, that for the $\pi h_{9/2}\otimes\nu i_{13/2}$ band would correspond to $\alpha^f_{p-n}=\alpha^f_p+\alpha^f_n=1/2+1/2=1$ (odd spin values). This phenomenon has been recently observed [8,9] and was explained in terms of a residual proton-neutron interaction. This so-called semidecoupled structure has been studied for many years and, as said, was detected in many nuclei throughout the rare-earth region and beyond, from Tm to Tl [1,4,5,8,9,45,50,51,61–63]. Due to one of the special features of this structure, namely that it starts with a number of low-energy highly converted $M1$ transitions, there always remained some uncertainty from an experimental point of view concerning the exact number of these transitions and hence the phase of the staggering also remained uncertain. It was assumed that the phase of the staggering conformed with the one predicted by the Coriolis interaction since no change of phase was observed in these bands until very recently [8,9]. The solution to this question [8,9] came ''from above,'' namely from the high-spin region of these bands through the accidental degeneracy with levels of other structures of known spins and parities. On the other hand, the possible role of a proton-neutron force in this structure was carefully analyzed many years ago [65] but the question remained open. The force used in that work was essentially the one obtained from the particle-hole multiplet $\pi h_{9/2}\otimes\nu^{-1}i_{13/2}$ in ^{208}Bi, renormalized by pairing correlations. This force has the following features. The matrix elements $\langle(j_pj_n^{-1})J|V_{p-n}|(j_pj_n^{-1})J\rangle=V_J^{-1}$ display small deviations ($\sigma\approx 60$ keV) around a mean of about 150 keV for the $J=5-10$ states, while the value for $J=11$, 886 keV is strongly repulsive, lying approximately 740 keV above the mean [10]. This number is large when compared to the energy of the 2^+ state in an even-even core of the region, taken as a measure of a typical collective rotational energy (at the beginning of a rotational band). So, the behavior of the system with $p-n$ force included is very similar to the

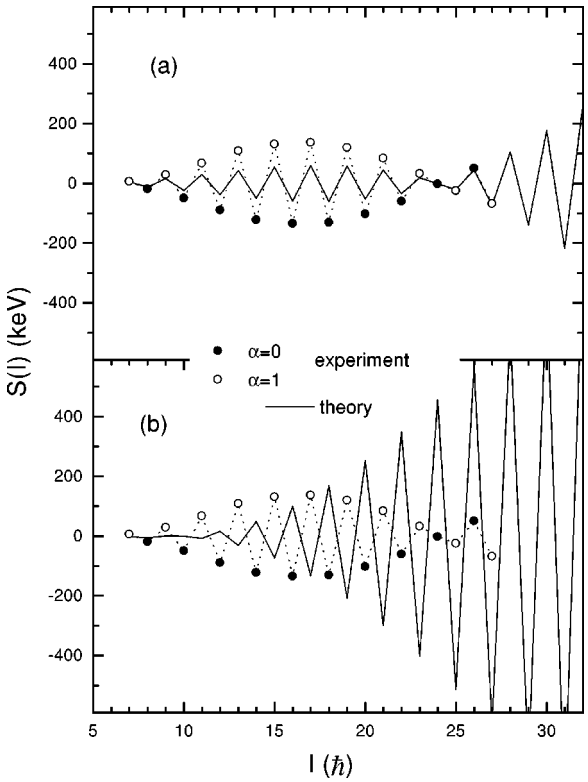

FIG. 17. Results of the two-quasiparticle-plus-rotor calculations with (a) and without (b) $p-n$ force. The experimental and calculated values $S(I)=E(I)-E(I-1)-[E(I+1)-E(I)+E(I-1)-E(I-2)]/2$ are plotted as a function of the angular momentum I.

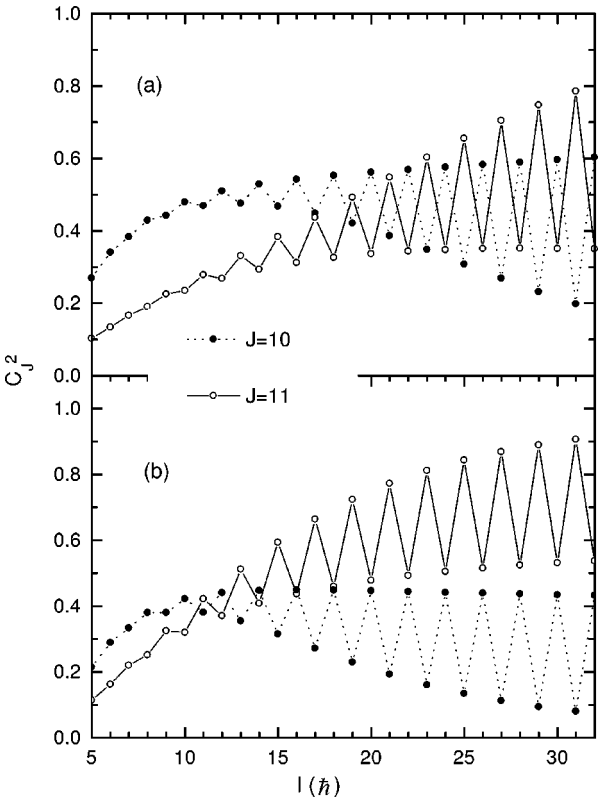

FIG. 18. Probability C_J^2 for $J=10$ and $J=11$ of finding the proton and neutron quasiparticles with intrinsic angular momentum coupled to $J=10$ and $J=11$, calculated with the two-quasiparticle-plus-rotor model with (a) and without (b) $p-n$ force as a function of the angular momentum I.

''noninteracting'' one except that the $J=11$ component is practically excluded from the spectrum of intrinsic excitations. Only when the rotational energy required to go from one state to the next one starts to become comparable to the intrinsic ($p-n$ interaction) energy required to maximally align proton and neutron (to $J=11$) will the change of phase occur. In this case one returns to a regime dominated by the Coriolis interaction and the phase of the staggering will become the ''normal'' one (namely here the $\alpha=1$, odd spin sequence will become favored). Figure 17 shows the result of a full two-quasiparticle-plus-rotor diagonalization within the $\pi h_{9/2}\otimes\nu i_{13/2}$, 70 element, configuration space ($\beta=0.24$, moment of inertia $J/\hbar^2=30$ MeV^{-1} and standard Nilsson parameters [32]) with, part (a), and without, part (b), $p-n$ force (the empirical ^{208}Bi force mentioned above). The ability of this calculation to reproduce the phenomenon is apparent, at least at a qualitative level. The point of the phase change is very well reproduced while the magnitude of the oscillation is underestimated. A better agreement would have to be considered fortuitous since the $p-n$ force has been treated in the single-j shell approximation. Only the matrix elements within the $\pi h_{9/2}\otimes\nu i_{13/2}$ configuration space have been taken into account while those between other components of the wave function have been neglected. In other words, the spherical ^{208}Bi force has only been renormalized by pairing correlations while the deformation effects were only taken into account through the splitting of the $\pi h_{9/2}$ and $\nu i_{13/2}$ multiplets. It should be pointed out, however, that the dominant components of the Nilsson wave functions are $\pi h_{9/2}$ and $\nu i_{13/2}$. In Ref. [8] a schematic central force of spatial-δ character with a spin-spin component was used. The relation between the purely spatial and spin-spin parts of the force is in fact fitted to the $p-n$ multiplets in spherical odd-odd nuclei and the overall strength parameter adopted [8] is not far from that obtained from the $\pi h_{9/2}\otimes\nu i_{13/2}$ multiplet in ^{208}Bi. Figure 18 shows the probability C_J^2, of finding the proton and neutron quasiparticles with intrinsic angular momentum coupled to $J=10$ or 11. (These calculations require a transformation from the strong coupling to the weak coupling basis, see Ref. [66]). It is apparent how the participation of the $J=11$ state is delayed in presence of the $p-n$ force. For high-spin states the structure of the favored states ($I=odd$) tends to be of the form $I=R+J=R+11$ ($R=even$ is the well defined, core angular momentum) both with and without the $p-n$ force. For low-spin states ($I<20\ \hbar$) in presence of the $p-n$ force the role of the $J=10$ component is dominant, so that favored states correspond to $I=even=R+J=R+10$ and unfavored states correspond to $I-1=odd=R+10-1$, namely the unstretched coupling between the core angular momentum and the intrinsic J. It is the interplay and competition between the Coriolis force (or the energy required to rotate) and the single (renormalized) $J=11$ $p-n$ matrix element which determines the signature phase inversion point. The $(-1)^I$ staggering is still a quantal feature related to the reflection symmetry of the core (which implies only even values of R) which translates into the $(-1)^I$ dependence of the Coriolis force acting, before the inversion point, on a system with $J_{\max}=10$, and

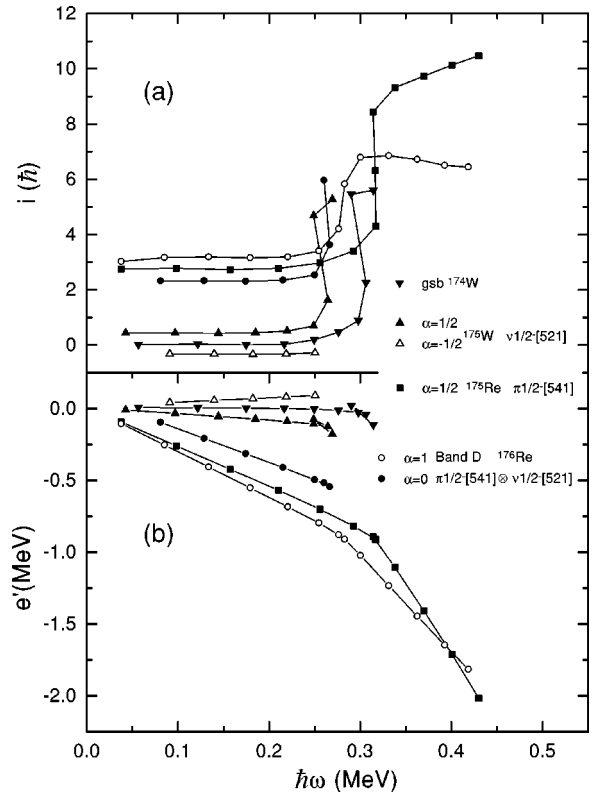

FIG. 19. Experimental alignments (a) and Routhians (b) as a function of the rotational frequency for the following structures: ground-state band of ^{174}W, $\nu 1/2^-[521]$ of ^{175}W, $\pi 1/2^-[541]$ of ^{175}Re and band D, $\pi 1/2^-[541]\otimes\nu 1/2^-[521]$, of ^{176}Re. The inertia parameters used for the reference configurations are reported in Table IV.

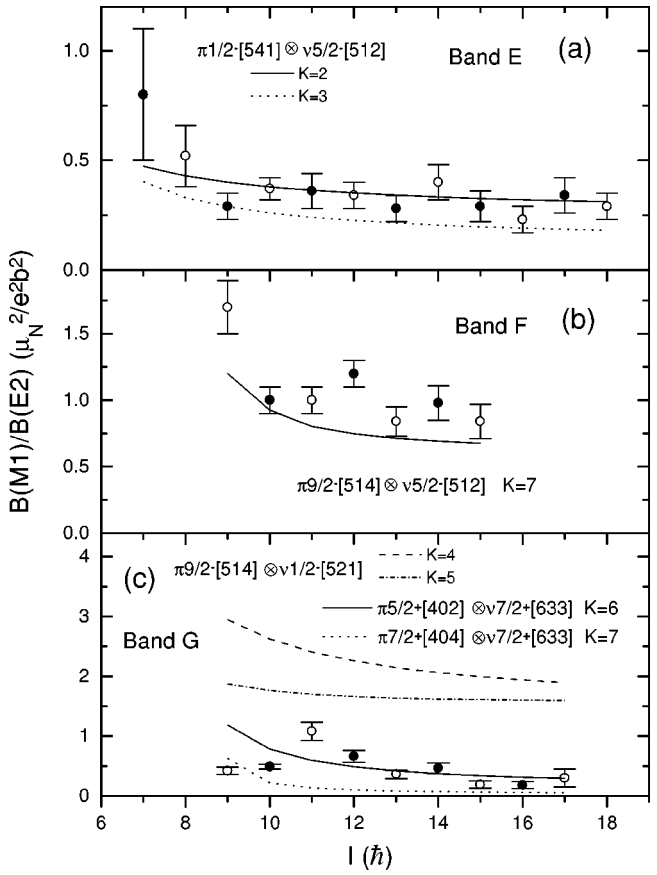

FIG. 20. Experimental $B(M1)/B(E2)$ values corresponding to bands E (a), F (b), and G (c) of ^{176}Re and the results of the calculations obtained in the framework of the cranking model for the indicated configurations. To plot the data for band E, $I_0=5$ was used (see text). Solid and open circles correspond to the $\alpha=0$ and $\alpha=1$ signature, respectively.

beyond the inversion point on a system with $J_{\max}=11$. Within this scenario the delay in crossing frequency observed in $\pi h_{9/2}$ bands of odd proton nuclei is understood in the following way. The crossing frequency at which the ground band Routhian is crossed by the S-band one is shifted to higher values because not only the energy to break an $i_{13/2}$ neutron pair is required but also the repulsive energy necessary to align to $J=11$ the $h_{9/2}$ quasiproton and one $i_{13/2}$ quasineutron has to be overcome.

C. Band D

Band D is a doubly decoupled band [4], of $\pi h_{9/2}(1/2^-[541])\otimes\nu 1/2^-[521]$ structure, having a 3^+ as band head. Results of this band have been discussed in previous work [11] in terms of the coupling between an aligned proton (i_p) to an aligned neutron pseudospin (of singlet type [67], $i_n=1/2$) which are coupled parallel ($i_{np}=i_p+1/2$, favored sequence) or antiparallel ($i_{np}=i_p-1/2$, unfavored sequence). The neutron orbital $1/2^-[521]$ is well described as a pseudospin singlet with quantum numbers: $1/2[\widetilde{420}]$. In Table IV the inertia parameters for both signatures of band D are listed, they were calculated using $K=0.5$ [11]. The values of the alignments before the backbending are also reported in comparison with the calculated ones from the odd particles. Figure 19(a) shows the alignment of band D vs the rotational frequency, the alignment of the core (^{174}W ground-state band), the neutron $1/2^-[521]$(^{175}W) and the proton $1/2^-[541]$ (^{175}Re) bands are also plotted. The crossing frequency was extracted from the Routhian vs frequency plot [Fig. 19(b)], this value can be understood by the combined effect of the $\pi h_{9/2}(1/2^-[541])$ which produces a delay and the $\nu 1/2^-[521]$ which in ^{175}W decreases the crossing frequency with respect to the even-even ^{174}W core (Table IV).

D. Bands C, E, F and G

Band C can be interpreted as a four-quasiparticle band, due to the uncertainties in spin and parity we were not able to identify its configuration.

Band E is strongly compressed, and the value of K extracted by the method described in Ref. [2] is $K=0.7$. The DCO values of the $\Delta I=1$ transitions correspond to negative mixing ratios. For example a $\delta=-0.10(7)$ was evaluated for the 149.1 keV transition of band E (Fig. 9). Among all the possible configurations expected in ^{176}Re (Table III) and not assigned to the previous discussed bands, negative mixing ratios are predicted for the $\Delta I=1$ transitions in the $\pi h_{9/2}(1/2^-[541])\otimes\nu 5/2^-[512]$ structure. Besides the $B(M1)/B(E2)$ calculated for this configuration give good fits to the experimental data for both values of $K=2$ and $K=3$ [Fig. 20(a)]. The presence of $\pi h_{9/2}$ can explain the compression and the low value extracted for K. This configura-

tion has recently been assigned to a relatively strongly populated band in ^{176}Ta [50] which also has in-band transitions with negative mixing ratios, and measured $B(M1)/B(E2)$ similar to those of band E. In ^{174}Ta a band with a sequence of very similar $\Delta I=1$ lines has been reported [9] as the $\pi 5/2^+[402]\otimes\nu 5/2^-[512]$ structure. For example the energies are: 98, 121, 146, and 168 keV in ^{174}Ta compared with 97.4, 122.0, 149.1, and 171.7 keV in ^{176}Re. For band E we discarded the $\pi 5/2^+[402]\otimes\nu 5/2^-[512]$ configuration because it has a positive δ and because it corresponds to a normal, high $K(=5)$ band. In ^{176}Ta the lowest observed state of the $\pi 1/2^-[541]\otimes\nu 5/2^-[512]$ structure has been assigned as (4^+), while in the ^{174}Lu [68] it is the 3^+ lying 19 keV below the 4^+. Difficulties were found in establishing the bandhead and the low-spin structure of band E, due to the compression of the band and the possibility of missing low-energy highly converted transitions. For the lowest observed level we propose $I_0^\pi=4^+$ or 5^+, from similarities with the bands in ^{174}Lu and ^{176}Ta.

Bands F and G are strongly linked between them, in a way that fixes their relative spins and the same parity for both bands. The values of K obtained by the method described in Ref. [2] are $K=7.85$ and $K=0.95$ for band F and G, respectively (a normal high K and a highly compressed band, respectively). Such a large value of K for band F suggests the possibility of the $\pi 9/2^-[514]\otimes\nu 5/2^-[512]$ configuration which moreover fits well the experimental in-band decay properties. The mixing ratios calculated with this configuration are positive (in agreement with the experiment) and around 0.4. Such non-negligible δ values were taken into account and the quantities $B(M1)/B(E2)(1+\delta^2)$ are compared favorably with experiment [Fig. 20(b)]. With this assignment the bandhead is the 7^+ state mentioned before as the level fed by the 99.5 keV which depopulates band A. This is in agreement with the bandhead energies predicted by the zero-order level scheme of ^{176}Re (Table III) which establishes the $7^+, \pi 9/2^-[514]\otimes\nu 5/2^-[512]$, bandhead at 326 keV$-186$ keV$=140$ keV below the $8^-, \pi 9/2^-[514]\otimes\nu 7/2^+[633]$ (band A).

For band G, from the zero-order level scheme (Table III) we can select the positive parity configurations not yet assigned: (i) $\pi 9/2^-[514]\otimes\nu 1/2^-[521]$, (ii) $\pi 5/2^+[402]\otimes\nu 7/2^+[633]$, and (iii) $\pi 7/2^+[404]\otimes\nu 7/2^+[633]$. Configurations (i) and (ii) imply missing transitions in the low-spin region since we assigned a (7^+) for the lowest observed state of band G, besides configuration (i) is not compressed. From the $B(M1)/B(E2)$ analysis, configurations (ii) and (iii) are the possible candidates for band G [Fig. 20(c)]. For the $\pi 7/2^+[404]\otimes\nu 7/2^+[633]$ the calculated mixing ratios have large values and in this case $B(M1)/B(E2)(1+\delta^2)$ was plotted. Taking into account the zero-order excitation energy the best candidate is configuration (ii).

IV. SUMMARY AND CONCLUSIONS

High-spin states in doubly odd ^{176}Re were investigated by means of in-beam γ-ray spectroscopy techniques using the multidetector array GASP. A wealth of rotational structures were identified and in most cases their structures (in terms of valence proton and neutron quasiparticle excitations) unambiguously assigned on the basis of qualitative features and quantitative parameters [like $B(M1)/B(E2)$]. Six out of nine predicted low-lying two-quasiparticle bands were significantly populated (excluding the $\pi 7/2^+[404]$ excitation which lies quite high in energy in Re). Signature inversion was established for both $\pi h_{11/2}\otimes\nu i_{13/2}$ and $\pi h_{9/2}\otimes\nu i_{13/2}$ structures. In particular the mechanism for this phenomenon is elucidated for the semidecoupled $\pi h_{9/2}\otimes\nu i_{13/2}$ band on the basis of an experimental $p-n$ force taken from ^{208}Bi and utilized in the same structure in the Tl region.

[1] A.J. Kreiner, M. Fenzl, S. Lunardi, and M.A.J. Mariscotti, Nucl. Phys. **A282**, 243 (1977).

[2] A.J. Kreiner, J. Davidson, M. Davidson, D. Abriola, C. Pomar, and P. Thieberger, Phys. Rev. C **36**, 2309 (1987); **37**, 1338 (1988).

[3] A. J. Kreiner, in *Proceedings of the International Conference on Contemporary Topics in Nuclear Structure Physics*, Cocoyoc, Mexico, 1988, edited by R. F. Casten, A. Frank, M. Moshinsky, and S. Pittel (World Scientific, Singapore, 1988), p. 521, and references therein.

[4] A.J. Kreiner, D. Di Gregorio, A.J. Fendrik, J. Davidson, and M. Davidson, Phys. Rev. C **29**, R1572 (1984); Nucl. Phys. **A432**, 451 (1985).

[5] A.J. Kreiner, J. Davidson, M. Davidson, P. Thieberger, E.K. Warburton, S. André, and J. Genevey, Nucl. Phys. **A489**, 525 (1988).

[6] A.J. Kreiner and M.A.J. Mariscotti, Phys. Rev. Lett. **43**, 1150 (1979).

[7] A.J. Kreiner and M.A.J. Mariscotti, J. Phys. G **6**, 13 (1980).

[8] R.A. Bark, J.M. Espino, W. Reviol, P.B. Semmes, H. Carlsson, I.G. Bearden, G.B. Hagemann, H.J. Jensen, I. Ragnarsson, L.L. Riedinger, H. Ryde, and P.O. Tjøm, Phys. Lett. B **406**, 193 (1997).

[9] R.A. Bark, H. Carlsson, S.J. Freeman, G.B. Hagemann, F. Ingebretsen, H.J. Jensen, T. Lönnroth, M.J. Piiparinen, I. Ragnarsson, H. Ryde, H. Schnack-Petersen, P.B. Semmes, and P.O. Tjøm, Nucl. Phys. **A630**, 603 (1998).

[10] J.P. Schiffer and W.W. True, Rev. Mod. Phys. **48**, 191 (1976).

[11] A.J. Kreiner, M.A. Cardona, H. Somacal, M.E. Debray, D. Hojman, J. Davidson, M. Davidson, D. De Acuña, D.R. Napoli, J. Rico, D. Bazzacco, R. Burch, S.M. Lenzi, C. Rossi Alvarez, N. Blasi, and G. Lo Bianco, Phys. Rev. C **50**, R530 (1994).

[12] G. Levinton, R. Pirchio, M. A. Cardona, M. Davidson, M. E. Debray, D. L. Hojman, A. J. Kreiner, H. Somacal, J. Davidson, D. De Acuña, D. R. Napoli, D. Bazzacco, S. M. Lenzi, P. Pavan, C. Rossi Alvarez, N. Blasi, and G. Lo Bianco, Annual Report 1994, LNL-INFN (Rep)-095/95, p. 63.

[13] D. Bazzacco, in Proceedings of the International Conference on Nuclear Structure at High Angular Momentum, Ottawa 1992 [Report No. AECL 10613 (unpublished)]; Vol. 2, p. 376.

[14] D. Santos, A.J. Kreiner, J. Davidson, M. Davidson, M.E. Debray, D. Hojman, and G. Falcone, Phys. Rev. C **39**, 902 (1989); J. Davidson, M. Davidson, M.E. Debray, G. Falcone, D. Hojman, A.J. Kreiner, I. Mayans, C. Pomar, and D. Santos, Z. Phys. A **324**, 363 (1986).

[15] A.O. Macchiavelli and E. Browne, Nucl. Data Sheets **69**, 903 (1993).
[16] E. Browne, Nucl. Data Sheets **60**, 227 (1990).
[17] R.A. Bark, G.B. Hagemann, B. Herskind, H.J. Jensen, W. Korten, J. Wrzesinski, H. Carlsson, M. Bergström, A. Brockstedt, A. Nordlund, H. Ryde, P. Bosetti, S. Leoni, F. Ingebretsen, and P.O. Tjøm, Nucl. Phys. **A591**, 265 (1995).
[18] V.S. Shirley, Nucl. Data Sheets **75**, 377 (1995).
[19] F. Rösel, H.M. Fries, K. Alder, and H.C. Pauli, At. Data Nucl. Data Tables **21**, 293 (1978).
[20] A. J. Kreiner, in *Proceedings of the XII Workshop on Nuclear Physics*, Cataratas del Iguazú, Argentina, 1989, edited by M. C. Cambiaggio, A. J. Kreiner, and E. Ventura (World Scientific, Singapore, 1989), p. 137.
[21] H. Carlsson, M. Bergströn, A. Brockstedt, L.P. Ekström, J. Lyttkens-Lindeén, H. Ryde, R.A. Bark, G.B. Hagemann, J.D. Garrett, R. Chapman, D. Clarke, F. Khazaie, J.C. Lisle, and J.N. Mo, Nucl. Phys. **A551**, 295 (1993).
[22] T. Shizuma, G. Sletten, R.A. Bark, I.G. Bearden, S. Leoni, M. Mattiuzzi, S. Mitarai, S.W. Ødegard, S. Skoda, K. Strähle, J. Wrzesinski, and Y.R. Shimizu, Nucl. Phys. **A626**, 760 (1997).
[23] V.S. Shirley, Nucl. Data Sheets **66**, 69 (1992).
[24] E. Browne, Nucl. Data Sheets **68**, 747 (1993).
[25] E. Browne, Nucl. Data Sheets **55**, 483 (1988); C. Baglin, *ibid.*, **68**, 747 (1993).
[26] R.B. Firestone, Nucl. Data Sheets **62**, 101 (1991).
[27] R.B. Firestone, Nucl. Data Sheets **65**, 589 (1992).
[28] C.J. Gallagher, Jr. and S.A. Moszkowski, Phys. Rev. **111**, 1282 (1958).
[29] F. Dönau and S. Frauendorf, in *Proceedings of the Conference on High Angular Momentum Properties of Nuclei*, Oak Ridge, 1982, edited by N. Johnson (Harwood Academic, Chur, Switzerland, 1982), p. 143.
[30] D. Hojman, A.J. Kreiner, M. Davidson, J. Davidson, M. Debray, E.W. Cybulska, P. Pascholati, and W.A. Seale, Phys. Rev. C **45**, 90 (1992).
[31] E. Browne, Nucl. Data Sheets **62**, 1 (1991).
[32] A. Bohr and B. Mottelson, in *Nuclear Structure* (Benjamin, Reading, MA, 1975), Vol. 2.
[33] J.A. Pinston, R. Bengtsson, E. Monnand, and F. Schussler, Nucl. Phys. **A361**, 464 (1981).
[34] R. Bengtsson, J.A. Pinston, E. Monnand, and F. Schussler, Nucl. Phys. **A389**, 158 (1982).
[35] J.A. Pinston, S. André, D. Barnéoud, C. Foin, and J. Genevey, Phys. Lett. **137B**, 47 (1984).
[36] S. Drissi, A. Bruder, J.-Cl. Dousse, V. Ionescu, J. Kern, J.-A. Pinston, S. Andréé, D. Barnéoud, J. Genevey, and H. Frisk, Nucl. Phys. **A451**, 313 (1986).
[37] M.A. Cardona, M.E. Debray, D. Hojman, A.J. Kreiner, H. Somacal, J. Davidson, M. Davidson, D. De Acuña, D.R. Napoli, J. Rico, D. Bazzacco, R. Burch, S.M. Lenzi, C. Rossi Alvarez, N. Blasi, and G. Lo Bianco, Z. Phys. A **354**, 5 (1996).
[38] A.J. Kreiner, M.A.J. Mariscotti, C. Baktash, E. der Mateosian, and P. Thieberger, Phys. Rev. C **23**, 748 (1981).
[39] M.A. Cardona, J. Davidson, D. Hojman, M.E. Debray, A.J. Kreiner, H. Somacal, J. Davidson, M. Davidson, D. De Acuña, D.R. Napoli, J. Rico, D. Bazzacco, R. Burch, S.M. Lenzi, C. Rossi Alvarez, N. Blasi, and G. Lo Bianco, Phys. Rev. C **56**, 707 (1997).
[40] S. Drissi, Z. Li, M. Délèze, J. Kern, and J.P. Vorlet, Nucl. Phys. **A600**, 63 (1996).
[41] Yunzuo Liu, Yingjun Ma, Hongting Yang, and Shangui Zhou, Phys. Rev. C **52**, 2514 (1995).
[42] D.M. Cullen, C.-H. Yu, D. Cline, M. Simon, D.C. Radford, M.A. Riley, and J. Simpson, Phys. Rev. C **57**, 2170 (1998).
[43] M.A. Lee, Nucl. Data Sheets **56**, 199 (1989).
[44] R.G. Helmer, Nucl. Data Sheets **64**, 79 (1991).
[45] G. Levinton *et al.* (unpublished).
[46] H. Zheng, Y-Z. Liu, Y-J. Ma, H-B. Sun, S-G. Zhou, H-T. Yang, J-D. Huo, X-A. Liu, Z-Y. Dai, X-G. Wu, S. Wen, G-J. Yuan, and C-X. Yang, J. Phys. G **23**, 723 (1997).
[47] K. Theine, C.-X. Yang, A.P. Byrne, H. Hübel, R. Chapman, D. Clarke, F. Khazaie, J.C. Lisle, J.N. Mo, J.D. Garrett, and H. Ryde, Nucl. Phys. **A536**, 418 (1992).
[48] Y.H. Zhang, S.Q. Zhang, Q.Z. Zhao, S.F. Zhu, H.S. Xu, X.H. Zhou, Y.X. Guo, X.G. Lei, J. Lu, Q.B. Gou, H.J. Jin, Z. Liu, Y.X. Luo, X.F. Sun, Y.T. Zhu, X.G. Wu, S.X. Wen, and C.X. Yang, Eur. Phys. J. A **1**, 119 (1998).
[49] D. Hojman *et al.* (unpublished).
[50] F.G. Kondev, G.D. Dracoulis, A.P. Byrne, and T. Kibédi, Nucl. Phys. **A632**, 473 (1998).
[51] A.J. Kreiner, V.R. Vanin, F.A. Beck, Ch. Bourgeois, Th. Byrski, D. Curien, G. Duchêne, B. Haas, J.C. Merdinger, M.G. Porquet, P. Romain, S. Rouabah, D. Santos, and J.P. Vivien, Phys. Rev. C **40**, R487 (1989).
[52] R. Bengtsson, H. Frisk, F.R. May, and J.A. Pinston, Nucl. Phys. **A415**, 189 (1984).
[53] I. Hamamoto, Phys. Lett. B **235**, 221 (1990).
[54] P.B. Semmes and I. Ragnarsson, in *Future Directions in Nuclear Physics with 4*Π *Gamma Detection Systems of the New Generation*, edited by J. Dudek and B. Haas, AIP Conf. Proc. 259 (AIP, New York, 1992), p. 566.
[55] K. Hara and Y. Sun, Nucl. Phys. **A531**, 221 (1991); K. Hara, *ibid.*, **A557**, 449c (1993).
[56] N. Yoshida, H. Sagawa, and J. Otsuka, Nucl. Phys. **A567**, 17 (1994).
[57] L.L. Riedinger, H.-Q. Jin, and C.-H. Yu, Nucl. Phys. **A520**, 287c (1990).
[58] K. E. G. Löbner, in *The Electromagnetic Interaction in Nuclear Spectroscopy*, edited by W. D. Hamilton (North-Holland, Amsterdam, 1975), p. 141.
[59] P.M. Walker, G.D. Dracoulis, A. Johnston, J.R. Leigh, M.G. Slocombe, and I.F. Wright, J. Phys. G **4**, 1655 (1978).
[60] G.D. Dracoulis, C. Fahlander, and A.P. Byrne, Nucl. Phys. **A401**, 490 (1983).
[61] A.J. Kreiner, D. Hojman, J. Davidson, M. Davidson, M. Debray, G. Falcone, D. Santos, C.W. Beausang, D.B. Fossan, E.S. Paul, R. Ma, S. Shi, and N. Xu, Phys. Lett. B **215**, 629 (1988).
[62] D. Hojman, A.J. Kreiner, and M. Davidson, Phys. Rev. C **46**, 1203 (1992).
[63] A.J. Kreiner, C. Baktash, G. García Bermúdez, and E. der Mateosian, Phys. Rev. Lett. **47**, 1709 (1981).
[64] A.J. Kreiner, Nucl. Phys. **A520**, 225 (1990).
[65] A.J. Kreiner, Phys. Rev. C **22**, 2570 (1980).
[66] A.J. Kreiner, Z. Phys. A **288**, 373 (1978).
[67] A.J. Kreiner, Phys. Lett. B **279**, 233 (1992), and references therein.
[68] A. Bruder, S. Drissi, V.A. Ionescu, J. Kern, and J.P. Vorlet, Nucl. Phys. **A474**, 518 (1987).